ITERATIVE PARTIALLY COHERENT DEMODULATION AND ITS APPLICATION TO FREQUENCY SHIFT KEY(FSK) MODULATED SIGNALS

By

OLUWATOSIN A. ADELADAN

A DISSERTATION PRESENTED TO THE GRADUATE SCHOOL
OF THE UNIVERSITY OF FLORIDA IN PARTIAL FULFILLMENT
OF THE REQUIREMENTS FOR THE DEGREE OF
DOCTOR OF PHILOSOPHY

UNIVERSITY OF FLORIDA

2012

To Jesus Christ, my parents and siblings, and to my Aduke

ACKNOWLEDGMENTS

I will like to thank Dr. John M. Shea for his mentorship, patience and guidance. I will also like to thank my parents and siblings for their prayers and support over the years. Finally, i will like to thank Aduke for her love and understanding during this phase of our lives.

TABLE OF CONTENTS

LIST OF TABLES

LIST OF FIGURES

Abstract of dissertation Presented to the Graduate School
of the University of Florida in Partial Fulfillment of the
Requirements for the Degree of Doctor of Philosophy

ITERATIVE PARTIALLY COHERENT DEMODULATION AND ITS APPLICATION TO FREQUENCY SHIFT KEY(FSK) MODULATED SIGNALS

By

Oluwatosin A. Adeladan

December 2012

Chair: John M. Shea
Major: Electrical and Computer Engineering

Demodulation schemes for information transmitted over communication channels are broadly classified into coherent or non-coherent schemes. For non-coherent demodulation, the knowledge of the channel is not available and the transmitted symbols are demodulated in its absence. For coherent demodulation, the channel is estimated and its influence is accounted for in demodulation. In cases where the channel estimate is poor, using this estimate for coherent demodulation can degrade the performance of the system. Partially coherent demodulation was introduced by Viterbi in 1965 as a way of exploiting the statistical information of the phase error with the goal of designing and implementing a better detector. However, not much work has been done in this area since its introduction. In particular, although iterative detection and decoding techniques are widely proposed for use in receivers, techniques to refine phase estimates and use these noisy phase estimates through partially coherent demodulation have not been considered prior to the work described in this dissertation. In this dissertation, we explore the use of partially coherent detection in conjunction with iterative channel estimation and demodulation in different channel scenarios. We show performance gains in terms of improved error rates, reduced error floor, and increased multi-user capability. We present results that show that these improvements translate to the MAC layer. We also present a new cross-layer technique that exploits information in the physical layer to optimize the aggregate system throughput in the MAC layer.

CHAPTER 1
INTRODUCTION

The rapidly increasing deployment of wireless technologies for both military and non-military applications necessitate the ability to communicate in increasingly challenging environments. The goal of living in a fully connected world has increased the demand for finite channel resources. It has also meant that devices have to be able to communicate in highly dynamic channels caused by fading.

Frequency hopping spread spectrum (FHSS) is one technology used to provide robustness against multiple access interference (MAI) and jamming. In slow FHSS systems, the packet to be transmitted is divided into different segments and each segment is transmitted in a different frequency channel according to a pseudo-random hopping pattern. The aim of this approach is to provide robustness to MAI by enabling signals to hop out of frequency channels that are impaired by interference or slow frequency-selective fading. However, when the hopping patterns of different transmitters are not orthogonal, packets from different transmitters collide at the receiver when they occupy the same frequency band at the same time. This event is known as a ”hit” [1, 2]. and it severely limits the multi-user capability of the system.

Most previous work on MAI mitigation in FHSS systems focuses on fast FHSS communication in which each symbol is sent over multiple frequencies [3–8]. In [9–11], joint detection of symbols have been considered for the slow FHSS case. In all of the previous work, it has been assumed that the hopping patterns and timing of the other users are known at the receiver. It has also been assumed that the receiver can simultaneously demodulate the signals at all the carrier frequencies, thus requiring a very wideband receiver. These assumptions produces complexity that prohibits their use in ad-hoc networks such as in the military SINCGARS [12] and Have Quick systems. Most of the work that have been done on improving the performance of frequency

hopping systems in ad hoc networks has focused on interference mitigation by erasing symbols that have been involved in a hit[13–15].

In [16], Viterbi characterized the probability density function (pdf) of the phase error arising from a phase-locked loop(PLL). The resulting pdf, known has the Tikhonov density, has been recently applied in the context of partially coherent demodulation to problems such as deriving the right strategies for decision fusion in large sensor networks [17], multipath diversity combining rules for RAKE receivers in direct sequence spread spectrum (DSSS) [18] and phase shift key modulated systems affected by inter symbol interference (ISI) [19]. In [20], partially coherent receiver architectures were derived for quadrature amplitude modulated (QAM) systems that show increased performance in bit error rates over a range of signal-to-noise ratios when compared to coherent demodulation.

In [21, 22], an expectation maximization(EM) based algorithm is used for channel estimation and signal detection in the presence of MAI for a system employing Binary Frequency Shift Keying (BFSK). This iterative algorithm uses noncoherent demodulation and takes advantage of the way that the symbols of the interfering and desired user are partially exposed when frequency shift keying is used and the symbols from different users arrive asynchronously at the receiver. In Chapter 2 of this Dissertation, we build upon this model by making proper use of the soft outputs of the decoder after each iteration to improve the channel estimates of the desired user. We also introduce the coherence parameter and show its derivation and application to partially coherent demodulation. We develop an interference mitigation scheme for the case of at most one strong interferer in each dwell interval and we assume that the complex channel gain of the interfering user can be easily estimated. We show that by using partially coherent demodulation [23–25] within an iterative receiver process in which the phase estimate of the desired user is refined, significant performance gains are achieved in terms of block error rates and the multi-user capability of the system.

Continuous phase frequency shift keying (CPFSK) is attractive as a modulation technique because it allows for a more efficient use of the bandwidth resource of the system than traditional FSK [23, 26]. However, CPFSK is not very robust to channel interference because of the inherent memory in the system. In previous work on FHSS systems that use CPFSK modulation, the multiple-access interference (MAI) is disregarded (essentially treating it as noise), which is shown to work well when the signal-to-interference ratio is high [27, 28]. In Chapter 3, we consider the problem of interference mitigation in an FHSS systems with non-orthogonal spreading sequences employing Binary Continuous Phase Frequency Shift Keying (BCPFSK). We develop an iterative interference mitigation scheme for a slow FHSS system employing BCPFSK and use the coherence parameter in channel estimation. This scheme addresses the difficulty posed by the non-memoryless nature of the modulation when it comes to estimating the channel parameters of the interfering user. In particular, because of the continuous phase requirement of CPFSK, this scheme is developed with the assumption that only the amplitude of the channel of the desired user can be estimated.

To enable coherent demodulation of CPFSK in a frequency non-selective time varying channel, pilot symbols are periodically inserted into the symbol sequence in order to track the channel. The pilot insertion rates are specified by the Nyquist Sampling theorem and depends on the fading rate of the channel [29]. In Chapter 4, we explore the use of sparser pilot symbol spacing and pilot insertion rates that are significantly lower than the rates specified by Nyquist and perform iterative channel estimation and demodulation based on quality of the channel estimates. We show that the adaptive nature of the partially coherent demodulation scheme allows for performance that is better than either coherent or noncoherent demodulation for most fading scenarios.

In Chapter 5, we study the performance improvement that is gained on the link layer by using interference mitigation at the physical layer. We also present a new cross

layer approach that uses local estimates at each node to dynamically adapt each node's transmission probability to enable the entire system to operate at close to its maximum achievable throughput.

Finally, we present conclusions in Chapter 6.

CHAPTER 2
INTERFERENCE MITIGATION WITH PARTIALLY COHERENT DEMODULATION IN A SLOW FREQUENCY-HOPPING SPREAD-SPECTRUM SYSTEM

2.1 Introduction of Interference Mitigation with Partially Coherent Demodulation in a Slow FHSS System

In [21, 22], an expectation maximization(EM) based algorithm for channel estimation and signal detection in the presence of MAI was presented for a system employing Binary Frequency Shift Keying (BFSK). The algorithm iterates among three stages: parameter estimation, interference and desired modulation symbol estimation (soft demodulation), and error correction and decoding stages. In this chapter, we revise the parameter estimation stage to make better use of the output of the soft decoder in estimating the parameters of the desired user. We also introduce a coherence parameter that will be used for partially coherent demodulation in the soft demodulation stage. We show how the performance of the system can be significantly improved by using partially coherent demodulation [23, 30]. Because the performance of the system also depends heavily on the impact of the dwell intervals hit by MAI, we investigate the effect of modeling the interference as Gaussian and estimating its variance across the dwell interval. We show that the channel variance estimate is also impacted by any error in the phase estimate, and updating the likelihoods based on the estimated channel variance can thus reduce the gains from partially coherent demodulation.

The rest of this chapter is organized as follows. In Section 2.2, we present the system and interference models. In Section 2.3, we present the channel estimation strategy using the EM algorithm. We explain how demodulation is performed in Section 2.4. Performance results are presented and discussed in Section 2.5 and the chapter is concluded in Section 2.6.

2.2 System Model

The system model to be considered is illustrated in Fig. 2-1. We consider a multiuser system with each user employing BFSK. At each user, the information is

encoded, interleaved and packed into a frame of length L coded bits. The frame is then divided into D dwell intervals of length L/D and passed through the modulator. Each symbol is then modulated with frequencies f_0 and f_1 if the corresponding bit is 0 and 1 respectively. The symbols in each dwell interval are then modulated onto a carrier according to a pseudo-random frequency-hopping scheme. Multiple access interference

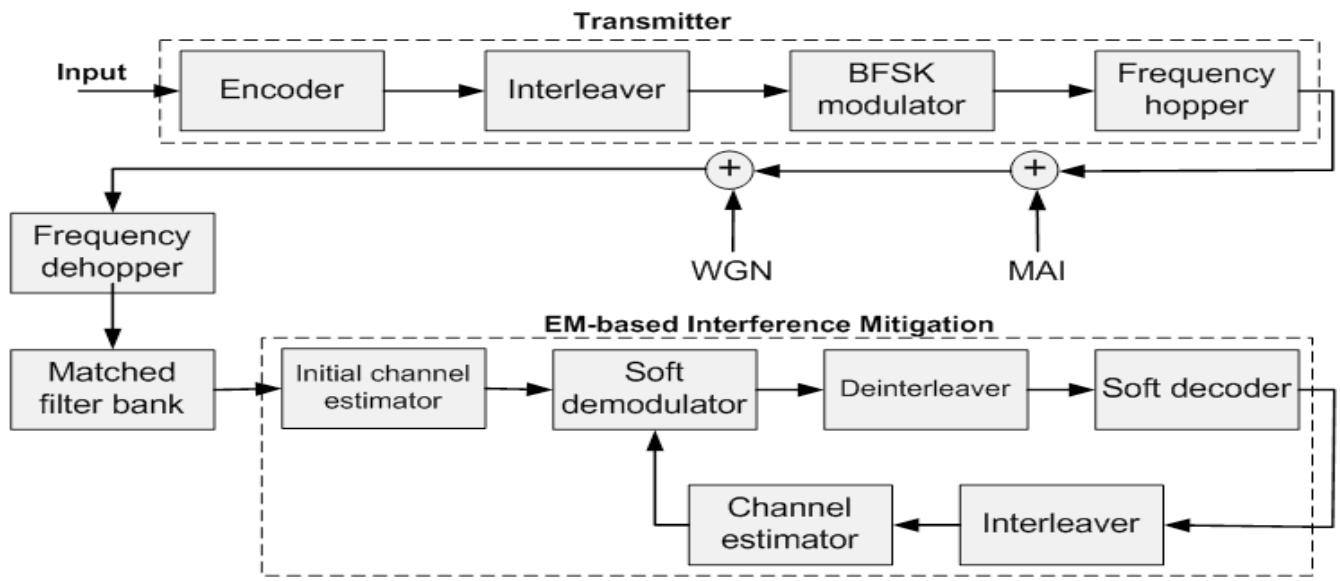

Figure 2-1. System model

occurs because the hopping patterns of the users are not orthogonal. We design an interference mitigation scheme based on the most likely scenario, in which there is one strong interferer in our dwell interval of interest. We consider a frequency-selective Rayleigh fading channel, which we model as a block fading channel with amplitudes and phases that are constant over each dwell interval but are independent across dwell intervals.

At the receiver, the signal is dehopped and passed through a bank of matched filters. The output of the matched filter is characterized by

$$y_k^0 = a_1(1 - x_k)e^{j\theta_1} + a_2 g_k(\tau)\, e^{j\theta_2} + n_0,$$

and

$$y_k^1 = a_1 x_k e^{j\theta_1} + a_2 h_k(\tau) e^{j\theta_2} + n_1, \tag{2–1}$$

where $A_1 = a_1 e^{j\theta_1}$ and $A_2 = a_2 e^{j\theta_2}$ are the complex-valued processes channel gains. Also, τ is the symbol-time offset between the interfering symbol and desired symbol, and $g_k(\tau)$ and $h_k(\tau)$ are the contributions of the interference signal to the desired signal at symbol k, which are defined as

$$g_k(\tau) = \frac{\tau}{T}\delta(I_{k-1}) + \left(1 - \frac{\tau}{T}\right)\delta(I_k),$$

and

$$h_k(\tau) = \frac{\tau}{T}\delta(I_{k-1} - 1) + \left(1 - \frac{\tau}{T}\right)\delta(I_k - 1).$$

Here I_{k-1} and I_k are values for consecutive interference symbols and $I_k = -1$ if no interference is present.

If we define

$$\begin{aligned}
\boldsymbol{y} &= (y_1^0, y_1^1, y_2^0, y_2^1, \ldots, y_N^0, y_N^1),\\
\boldsymbol{\lambda} &= (a_1, a_2, \theta_1, \theta_2, \tau),\\
\boldsymbol{x} &= (x_1^0, x_1^1, x_2^0, x_2^1, \ldots, x_N^0, x_N^1), \text{ and}\\
\boldsymbol{I} &= (I_1, I_2, I_3, \ldots, I_N),
\end{aligned}$$

then, the probability likelihood function of $\boldsymbol{y}$ given $\boldsymbol{\lambda}$,$\boldsymbol{x}$ and $\boldsymbol{I}$ is given by

$$\begin{aligned}
p(y_k^0, y_k^1|\boldsymbol{x}, \boldsymbol{I}, \boldsymbol{\lambda}) = \frac{1}{4\pi^2\sigma^4} \exp\left(-\frac{1}{2\pi\sigma^2}\left|y_k^0 - a_1(1 - x_k)e^{j\phi_1} - a_2 g_k(\tau)e^{j\phi_2}\right|^2\right)\\
\times \exp\left(-\frac{1}{2\pi\sigma^2}\left|y_k^1 - a_1(x_k)e^{j\phi_1} + a_2 h_k(\tau)e^{j\phi_2}\right|^2\right).
\end{aligned} \tag{2–2}$$

2.3 Channel Estimation

2.3.1 Expectation Maximization (EM) Algorithm

The channel parameters, $\boldsymbol{\lambda}$, are estimated iteratively using the EM algorithm. We treat the symbols of the desired user and the interfering user as the unobserved latent data. The algorithm updates the estimate from the equation,

$$\boldsymbol{\lambda}^{(n)} = \text{ arg max}_{\boldsymbol{\lambda}} \, Q(\boldsymbol{\lambda}, \boldsymbol{\lambda}^{(n-1)}), \tag{2–3}$$

where $Q(\boldsymbol{\lambda}, \boldsymbol{\lambda}^{(n-1)})$ is Baum's auxiliary function, given by

$$Q(\boldsymbol{\lambda}, \boldsymbol{\lambda}^{'}) = E\left[\text{log } p(\boldsymbol{y}, \boldsymbol{x}, \boldsymbol{I}|\boldsymbol{\lambda})|\boldsymbol{y}, \boldsymbol{\lambda}'\right] = \\ E\left[\text{log } p(\boldsymbol{y}|\boldsymbol{\lambda})|\boldsymbol{y}, \boldsymbol{\lambda}'\right] + E\left[\text{log } p(\boldsymbol{x}|\boldsymbol{\lambda})|\boldsymbol{y}, \boldsymbol{\lambda}'\right] + E\left[\text{log } p(\boldsymbol{I}|\boldsymbol{\lambda})|\boldsymbol{y}, \boldsymbol{\lambda}'\right] \tag{2–4}$$

Since $\boldsymbol{I}$ and $\boldsymbol{x}$ are assumed to be independent of our channel parameters, (2–4) can be written as

$$Q(\boldsymbol{\lambda}, \boldsymbol{\lambda}^{'}) = C - \frac{1}{N}\sum_{k=1}^{N}\sum_{x_k, I_{k-1}, I_k}\left[\frac{1}{2\pi\sigma^2}\left(\left|y_k^0 - a_1(1-x_k)e^{j\theta_1} - a_2 g_k(\tau)e^{j\theta_2}\right|^2\right.\right. \\ \left.\left. + \left|y_k^1 - a_1(x_k)e^{j\theta_1} + a_2 h_k(\tau)e^{j\theta_2}\right|^2\right) \times p(x_k|y_k, \boldsymbol{\lambda}')p(I_{k-1}, I_k|y_k, \boldsymbol{\lambda}')\right], \tag{2–5}$$

where C is the combination of all parameters that are independent of $\boldsymbol{\lambda}$; as such, only the second term is useful for maximization. Also. let

$$Q_k(\boldsymbol{\lambda}, \boldsymbol{\lambda}^{'}) = \sum_{x_k, I_{k-1}, I_k}\left[\frac{1}{2\pi\sigma^2}\left(\left|y_k^0 - a_1(1-x_k)e^{j\theta_1} - a_2 g_k(\tau)e^{j\theta_2}\right|^2\right.\right. \\ \left.\left. + \left|y_k^1 - a_1(x_k)e^{j\theta_1} + a_2 h_k(\tau)e^{j\theta_2}\right|^2\right) \times p(x_k|y_k, \boldsymbol{\lambda}')p(I_{k-1}, I_k|y_k, \boldsymbol{\lambda}')\right] \tag{2–6}$$

and

$$Q(\boldsymbol{\lambda}, \boldsymbol{\lambda}^{'}) = \sum_{k=1}^{N} Q_k(\boldsymbol{\lambda}, \boldsymbol{\lambda}^{'}). \tag{2–7}$$

To find the channel parameters that maximize (2–5), we define the gradient operator $\nabla_x = \frac{\delta x}{\delta u} + j\frac{\delta x}{\delta v}$ for $x = u + jv$. The locally optimal value of $\boldsymbol{\lambda}_k$ can be found by solving the following set of equations

$$\nabla_{A_1} Q_k(\boldsymbol{\lambda}, \boldsymbol{\lambda}') = 0, \text{ and} \tag{2–8}$$

$$\nabla_{A_2} Q_k(\boldsymbol{\lambda}, \boldsymbol{\lambda}') = 0. \tag{2–9}$$

Solving (2–8) and (2–9) produces the following set of linear equations

$$\beta_1 \hat{A}_{1k} + \beta_2 \hat{A}_{2k} = \rho_1, \text{ and} \tag{2–10}$$

$$\beta_3 \hat{A}_{1k} + \beta_4 \hat{A}_{2k} = \rho_2. \tag{2–11}$$

where

$$\begin{aligned}
\beta_1 &= 1, \\
\beta_2 &= \sum_{x_k} \sum_{I_{k-1}} \sum_{I_k} \left\{ \left[(1 - x_k) g_k(\tau) + x_k h_k(\tau) \right] p(x_k | \boldsymbol{y}, \boldsymbol{\lambda}') p(I_{k-1}, I_k | \boldsymbol{y}, \boldsymbol{\lambda}') \right\}, \\
\beta_3 &= \beta_2, \\
\beta_4 &= \sum_{I_{k-1}} \sum_{I_k} \left\{ g_k(\tau)^2 + h_k(\tau)^2 \right\} p(I_{k-1}, I_k | \boldsymbol{y}, \boldsymbol{\lambda}'), \\
\rho_1 &= \sum_{x_k} \left[(1 - x_k) y_k^0 + x_k y_k^1 \right] p(x_k | \boldsymbol{y}, \boldsymbol{\lambda}'), \quad \text{and} \\
\rho_2 &= \sum_{I_{k-1}} \sum_{I_k} \left\{ g_k(\tau) y_k^0 + h_k(\tau) y_k^1 \right\} p(I_{k-1}, I_k | \boldsymbol{y}, \boldsymbol{\lambda}').
\end{aligned} \tag{2–12}$$

We can rewrite (2–10) and (2–11) in matrix form as

$$\boldsymbol{\beta} \hat{\boldsymbol{A}}_{\boldsymbol{k}} = \boldsymbol{\rho}. \tag{2–13}$$

From (2–15), all the elements of $\boldsymbol{\beta}$ are greater than or equal to zero. It then follows that the determinant of $\boldsymbol{\beta}$ denoted $|\boldsymbol{\beta}| \to 0$ as $\beta_2, \beta_4 \to 0$. This is the special case for which it has been determined that there are no interference components in the same branch as the desired user for that particular symbol. Here, $\hat{A}_{1k} = \rho_1$.

The estimate of A_1 over a particular dwell interval is given by

$$\hat{A}_1 = \sum_{k=1}^{N} \hat{A}_{1k}.$$

We also generate estimates of the variance, σ_c, of $\hat{A}_1$. The estimate of the offset between the desired and interfering user is given by

$$\nabla_\tau Q(\boldsymbol{\lambda}, \boldsymbol{\lambda}') = 0, \tag{2–14}$$

whose solution is of the form

$$\upsilon_1\left(\frac{\tau}{T}\right) = \upsilon_2 - \upsilon_3,$$

and

$$\begin{aligned}
\upsilon_1 &= \sum_k \sum_{I_{k-1}} \sum_{I_k} |A_2|^2 \left[(\delta(I_{k-1}) - \delta(I_k))^2 + (\delta(I_{k-1}-1) - \delta(I_k-1))^2\right] p(I_{k-1}, I_k|\boldsymbol{y}, \boldsymbol{\lambda}'), \\
\upsilon_2 &= \sum_k \sum_{I_{k-1}} \sum_{I_k} \sum_{x_k} \left[\mathrm{Re}\left\{A_2(\delta(I_{k-1}) - \delta(I_k))(y_k^{0*} - A_1^*(1-x_k))\right\} + \right. \\
&\qquad \left. \mathrm{Re}\left\{A_2(\delta(I_{k-1}-1) - \delta(I_k-1))(y_k^{1*} - A_1^* x_k)\right\}\right] p(x_k|\boldsymbol{y}, \boldsymbol{\lambda}') p(I_{k-1}, I_k|\boldsymbol{y}, \boldsymbol{\lambda}'), \\
\upsilon_3 &= \sum_k \sum_{I_{k-1}} \sum_{I_k} |A_2|^2 \left[(\delta(I_{k-1}) - \delta(I_k))\delta(I_k) + (\delta(I_{k-1}-1) - \delta(I_k-1))\delta(I_k-1)\right] \\
&\qquad p(I_{k-1}, I_k|\boldsymbol{y}, \boldsymbol{\lambda}').
\end{aligned} \tag{2–15}$$

2.3.2 Coherence Parameter Estimation

Given estimates of the variance, σ_c, of $\hat{A}$, we map between the SNR($|A_1|^2/\sigma_c^2$) and coherence parameter, α, using the following approach. Consider a received signal whose lowpass I and Q components, y_I and y_Q, have been corrupted by uncorrelated Gaussian noise with variance σ_n, it follows that we can write the joint pdf of both components as

$$p(y_I, y_Q) = \frac{1}{2\pi\sigma^2} \exp\left(-\frac{(y_I - A_{1I}\sqrt{E})^2 + (y_Q - A_{1Q}\sqrt{E})^2}{2\sigma^2}\right),$$

where $A_{1I}\sqrt{E}$ and $A_{1Q}\sqrt{E}$ are the in-phase and quadrature channel effects normalized by the symbol energy. If we define

$$Y = \sqrt{y_I^2 + y_Q^2}$$

and

$$\theta = \arctan \frac{y_Q}{y_I}.$$

It follows that after some substitution that the joint pdf of the magnitude, Y, and phase, θ, is given by

$$p(Y,\theta) = \frac{Y}{2\pi\sigma_n^2} \exp\left(-\frac{Y^2 - 2Y|A_1|\cos(\angle A - \theta)\sqrt{E} + |A_1|^2 E}{2\sigma_n^2}\right), \tag{2–16}$$

where the $\psi = \angle A - \theta$ is the phase error.

For ease of exposition, let us define $\mu = |A_1|^2 E$, it then follows that we can write the marginal pdf of the phase as

$$\int_0^\infty p(Y,\psi)dY = \frac{1}{2\pi\sigma^2} \exp\left(-\frac{\mu}{2\sigma^2}\right) \int_0^\infty Y \exp\left(\frac{2Y\cos\psi - Y^2}{2\sigma^2}\right) dY. \tag{2–17}$$

After some manipulations, we can express (2–17) as

$$p(\psi) = \frac{1}{2\pi\sigma^2} \exp\left(-\frac{\mu}{2\sigma^2}\right) \exp\left(\frac{\mu^2\cos^2\psi}{2\sigma^2}\right) \times \left(\int_0^\infty \mu\cos\psi \exp\left(-\frac{(Y-\mu\cos\psi)^2}{2\sigma^2}\right) dY + \int_0^\infty (Y-\mu\cos\psi) \exp\left(-\frac{(Y-\mu\cos\psi)^2}{2\sigma^2}\right) dY\right). \tag{2–18}$$

If we define $u = \frac{(Y-\mu\cos\psi)^2}{2\sigma^2}$ and apply this change of variable to the second integral term, we get

$$p(\psi) = \frac{1}{2\pi\sigma^2} \exp\left(-\frac{\mu^2}{2\sigma^2}\right) \exp\left(\frac{\mu^2\cos^2\psi}{2\sigma^2}\right) \times \left(\int_0^\infty \mu\cos\psi \exp\left(-\frac{(Y-\mu\cos\psi)^2}{2\sigma^2}\right) dY + \int_{\mu^2\cos^2\psi/(2\sigma^2)}^\infty \exp(-u)\, du\right). \tag{2–19}$$

This expression reduces to

$$p(\psi) = \exp\left(-\frac{\mu^2}{2\sigma^2}\right)\exp\left(\frac{\mu^2\cos^2\psi}{2\sigma^2}\right)\times$$
$$\left(\frac{\mu\cos\psi}{\sqrt{2\pi\sigma^2}}\int_0^\infty \frac{1}{\sqrt{2\pi\sigma^2}}\exp\left(-\frac{(Y-\mu\cos\psi)^2}{2\sigma^2}\right)dY + \frac{1}{2\pi\sigma^2}\exp\left(-\frac{\mu^2\cos^2\psi}{2\sigma^2}\right)\right). \quad (2\text{–}20)$$

Expanding and writing in terms of the Q-function, we get

$$p(\psi) = \frac{\mu\cos\psi}{\sqrt{2\pi\sigma^2}}\exp\left(-\frac{\mu^2}{2\sigma^2}\right)\exp\left(\frac{\mu^2\cos^2\psi}{2\sigma^2}\right)\left(1-Q\left(\frac{\mu\cos\psi}{\sigma}\right)\right)+\frac{1}{2\pi\sigma^2}\exp\left(-\frac{\mu^2}{2\sigma^2}\right). \quad (2\text{–}21)$$

Using the fact that $Q(x) \approx \exp(-x^2/2)$ for large values of x, we can re-write (2–21) as

$$p(\psi) \approx \frac{\mu\cos\psi}{\sqrt{2\pi\sigma^2}}\exp\left(-\frac{\mu^2}{2\sigma^2}\right)\exp\left(\frac{\mu^2\cos^2\psi}{2\sigma^2}\right)\left(1-\exp\left(-\frac{\mu^2\cos^2\psi}{2\sigma^2}\right)\right)+\frac{1}{2\pi\sigma^2}\exp\left(-\frac{\mu^2}{2\sigma^2}\right). \quad (2\text{–}22)$$

The second term goes to zero for high SNRs, so that we have

$$p(\psi) \approx \frac{\mu\cos\psi}{\sqrt{2\pi\sigma^2}}\exp\left(-\frac{\mu^2}{2\sigma^2}\right)\exp\left(\frac{\mu^2\cos^2\psi}{2\sigma^2}\right). \quad (2\text{–}23)$$

This can be re-written as

$$p(\psi) \approx \frac{\mu\cos\psi}{\sqrt{2\pi\sigma^2}}\exp\left(\frac{\mu^2}{2\sigma^2}\left(\cos^2\psi-1\right)\right) \quad (2\text{–}24)$$

For large μ^2/σ^2, the density is concentrated around zero for which $\cos\psi = 1$, so, we can re-write the expression as

$$p(\psi) \approx \frac{\mu}{\sqrt{2\pi\sigma^2}}\exp\left(-\frac{\mu^2}{2\sigma^2}\sin^2\psi\right). \quad (2\text{–}25)$$

This is the Tikhonov density presented in (2–26)[16, 23] at high SNRs. Let ψ denote the random channel phase, the probability density function for ψ is

$$p(\psi|\hat{\psi}) = \frac{\exp\left(\alpha\cos\psi\right)}{2\pi\,\mathrm{I}_0(\alpha)}, \quad |\psi| \le \pi \quad (2\text{–}26)$$

where $\mathrm{I}_0(\cdot)$ is the modified Bessel function of the first order.

For large values of α, the Bessel function in the denominator can be approximated as

$$\mathrm{I}_0(\alpha) \approx \frac{\exp \alpha}{\sqrt{2\pi\alpha}},$$

and (2–26) can be modified to produce

$$p(\psi) = \frac{\exp\left(\alpha \cos \psi\right)}{2\pi\, \mathrm{I}_0(\alpha)} \approx \frac{\sqrt{\alpha} \exp\left(\alpha\left(\cos \psi - 1\right)\right)}{\sqrt{2\pi}} = \frac{\sqrt{\alpha} \exp\left(-2\alpha \sin^2(\psi/2)\right)}{\sqrt{2\pi}}$$

The pdf is concentrated around $\psi = 0$ for large values of α. In this case, $\sin^2(\psi/2) \approx (\sin^2 \psi)/4$. The resulting expression is given by

$$p(\psi) = \frac{\sqrt{\alpha} \exp\left(-\frac{1}{2}\alpha \sin^2(\psi)\right)}{\sqrt{2\pi}}. \tag{2–27}$$

Comparing Equation 2–25 and Equation 2–27, it is quite straightforward to see the equivalence. Also, $\alpha = \mu^2/\sigma^2$ for high signal to noise ratios.

We can also see from (2–26) that when α is zero, the resulting probability density function (pdf) degenerates to a uniform distribution, which corresponds to noncoherent detection. On the other hand, the expression becomes a delta function as $\alpha \to \infty$, which corresponds to coherent detection.

Let $\boldsymbol{\psi} = \left[\psi^1, \psi^2, ..., \psi^N\right]$ and define $\mu_k = \psi_k - \hat{\psi}, 1 \leq k \leq N$. It then follows that the joint pdf of $\boldsymbol{\psi}$ given α and the μ_k's is given by

$$p(\psi|\hat{\boldsymbol{\psi}}, \alpha) = \prod_{k=1}^{N} \frac{\exp(\alpha \cos(\mu_k))}{2\pi\, \mathrm{I}_0(\alpha)}, \qquad |\mu_k| \leq \pi. \tag{2–28}$$

The Maximum-Likelihood(ML) estimate of α satisfies

$$\frac{d}{d\alpha}\prod_{k=1}^{N}\frac{\exp(\alpha\cos(\mu_k))}{2\pi\,\mathrm{I}_0(\alpha)} = 0.$$

$$\equiv [2\pi\,\mathrm{I}_0(\alpha)]^N \sum_{k=1}^{N}\cos(\mu_k)\exp\left[\alpha\sum_{k=1}^{N}\cos(\mu_k)\right]$$

$$-\exp\left[\alpha\sum_{k=1}^{N}\cos(\mu_k)\right](2\pi)^N N\,\mathrm{I}_0(\alpha)^{N-1}\,\mathrm{I}_1(\alpha) = 0. \quad (2\text{–}29)$$

After some simplification, we get that the ML estimate of α satisfies

$$\frac{1}{N}\sum_{k=1}^{N}\cos(\mu_k) = \frac{\mathrm{I}_1(\alpha)}{\mathrm{I}_0(\alpha)}. \quad (2\text{–}30)$$

We utilize an empirical approach to map between the parameters of the Gaussian channel and the coherence parameter α in the Tikhonov distribution using (2–30). We generate $N = 10^8$ channel realizations for each value of SNR with known symbols in order to investigate the relationship between the SNR of the channel and the coherence parameter. These values were compiled and stored in a table. Fig. 2-2 shows this relationship for a limited range of SNR values. Table 2-1 gives us values of the coherence parameter at selected points.

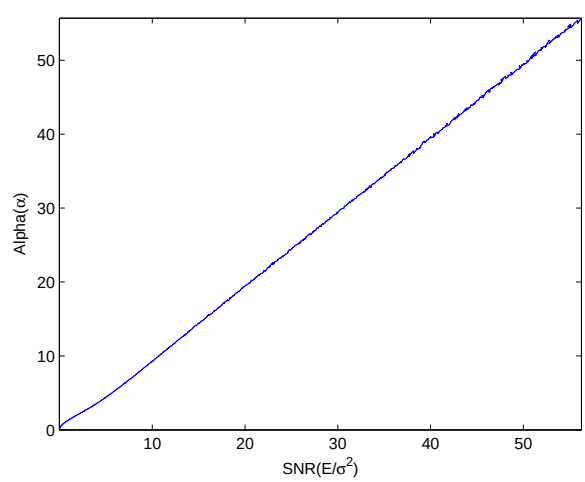

Figure 2-2. Graph of the coherence parameter (α) vs. SNR (E/σ^2) .

Table 2-1. Selected values of SNR and corresponding α.

SNR(E/σ^2)	Coherence parameter(α)
200	199.5512
100	99.5072
20	19.4182
10	9.2941
5	4.4061
1	1.3514

2.3.3 Initial Channel Estimation

2.3.3.1 The one interferer case

Due to the absence of the required probabilities at the beginning of the iteration process, we generate local estimates of A_1 for each symbol in the dwell interval according to

$$\hat{A}_{1k} = y_k^0 + y_k^1.$$

With these local estimates, we attempt to reduce the effect of the interferer by observing the median of the local estimates within a dwell interval and setting our estimate of A_1 to this median. Additionally, we also estimate the variance of the channel, with the purpose of quantifying the quality of our estimate and the channel, using the median as the de facto mean.

The addition of K null symbols at the beginning and end of the dwell interval assists in the estimation of the interfering user parameters. K null symbols are also inserted in punctured positions within the frame. The decision statistic of a null symbol containing interference can be written as

$$z_k^0 = A_2 g_k(\tau) + n_0,$$

and

$$z_k^1 = A_2 h_k(\tau) + n_1, 1 \geq k \geq K.$$

The maximum likelihood estimate of A_2 is derived for a set of K null bits by maximizing

$$\begin{aligned} J(A_2) = & \ \log P(z_1^0, z_1^1, z_2^0, z_2^1, z_3^0, z_3^1, ..., z_K^0, z_K^1 | I, \lambda) \\ = & \ C_1 - \frac{1}{N_0} \sum_{k=1}^{K} \left(\left| z_k^0 - A_2 g_k(\tau) \right|^2 + \left| z_k^1 - A_2 h_k(\tau) \right|^2 \right), \end{aligned}$$

whose solution is

$$\hat{A}_2 = \frac{\sum_{k=1}^{K} \left(z_k^0 g_k(\tau) + z_k^1 h_k(\tau) \right)}{\sum_{k=1}^{K} \left(g_k^2(\tau) + h_k^2(\tau) \right)}.$$

Since we have no prior information about the contributions of the interferer in the first iteration, we set $h_k(\tau) = g_k(\tau) = \frac{1}{2}$, so that our estimate becomes

$$\hat{A}_2 = \frac{1}{K} \sum_{k=1}^{K} \left(z_k^0 + z_k^1 \right). \tag{2–31}$$

We use (2–31) to generate three estimates of A_2 using the left, right and the random null bits. We choose the estimate that has the maximum amplitude and use this as the estimate of the channel parameter of our interferer.

2.3.3.2 The multiple interferer case

Since it is widely understood that the EM algorithm is very sensitive to initial conditions, obtaining the best possible initial channel estimate is of utmost importance. If there are more than one interferer in a dwell interval, then the estimates of the parameters of the interference should vary over the dwell interval. Consider a case where we have 100 users contending over 100 frequency bands. The probability that a particular dwell interval will be hit by more than one interferer is 0.2605, which implies that more than a quarter of dwell intervals will be hit by more than one interferer.

For these dwell intervals, our assumption of a constant interference gain in a dwell interval does not hold. To deal with this scenario, we derive the channel estimate by following these steps

1.) We derive two estimates of the interferer(s) using the left and right null bits.

2.) Using both the left and the right null bits, we generate two estimates of the desired user gain using the first K symbols after the left null bits and the last K symbols before the right null bits. We also generate variance estimates for both cases.

3.) We choose the estimate of the desired user's channel gain with the least variance and subtract it from the received symbols to give estimates of the interference at each symbol position.

4.) Because these estimates are prone to be noisy, we pass the stream of estimates through a moving average filter to estimate the channel parameter of the interfering user at each symbol position.

2.4 Soft Demodulator and Decoder

In this section, we present a trellis based algorithm that is used to calculate the probabilities of the desired and interfering symbols that are used by the channel estimation presented in the last section as well as the error-correction decoder. The soft demodulator utilizes extrinsic information fed back from the decoder (the symbol probabilities) as well as intrinsic information that it generates from the trellis. The trellis

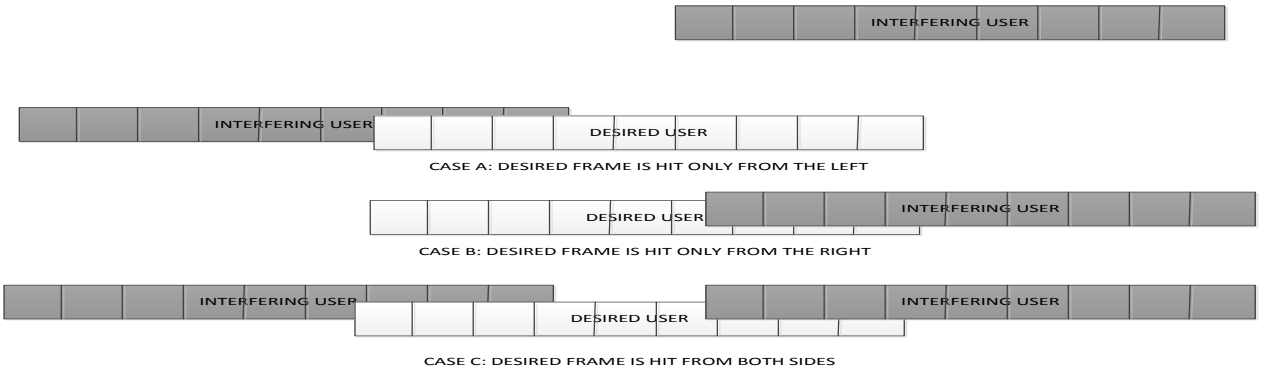

Figure 2-3. Interference patterns

is designed to be able to handle at least one strong interferer in each dwell interval. When a dwell interval is hit by interference from a single user, the resulting interference can be classified as fitting one of three patterns. The dwell interval could be be hit from the left, the right, or both sides (Fig. 2-3). Also, because of the asynchronous nature of the transmission, a desired symbol that has been hit may contain interference from two consecutive symbols from the interfering signal. We refer to the earlier and later symbols as the left- and right-interfering symbols, respectively.

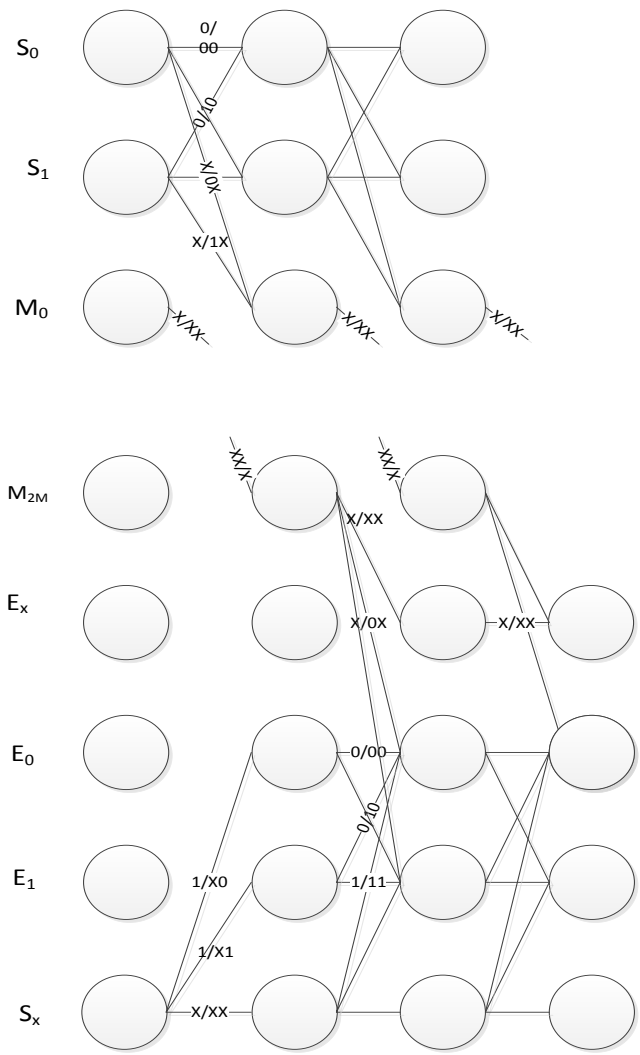

Figure 2-4. Trellis used in the BCJR algorithm for the soft demodulator.

Fig. 2-4 gives a pictorial representation of the trellis used. The trellis starts in states S_0, S_1, or S_X. When the desired frame is hit from the left, the trellis starts in states S_0 or S_1 with the subscripts representing the value of the left-interfering symbol. The trellis starts from S_X if the dwell interval has not been hit from the left. Once in states S_0 or S_1, the trellis can transition to either state S_0 or S_1, depending on the value of the next interference symbol, or to state M_1 when the interference from the left terminates. There are $2K$ states $M_1, M_2, ..., M_{2K}$ used to enforce the presence of $2K$ null symbols between dwell intervals.

State M_{2K} transitions to states E_0 or E_1 if the dwell interval is hit from the right or state E_X if there is no interference from the right. If there is no hit from the left, state S_X also transitions to E_0 or E_1 if there is a hit from the right. In total, the trellis contains $2K + 6$ states.

The branch input to the trellis is the interference symbol which takes its value from the set $\{0, 1, X\}$ which represent interference value 0, interference value 1, and no interference. The input transitions the trellis into one of the states whose subscript is the input value. For example, an input value of 0 transitions the trellis into states S_0 or E_0; an input of 1 to states S_1 or E_1; and an input of X to either S_X, E_X or one of the other $2K$ states.

We use the trellis to calculate the probabilities of the desired and interfering symbols using the BCJR algorithm. The branch metric connecting state s' at time $k-1$ to s at time k is given by

$$\begin{aligned}\gamma_k(s', s) &= p(y_k^0, y_k^1, s_k = s | s_{k-1} = s') = p(y_k^0, y_k^1 | s_k = s, s_{k-1} = s') p(s_k = s | s_{k-1} = s') \\ &= \left\{ \sum_{x_k} p\left[y_k^0, y_k^1 | I_{k-1}(s_{k-1}), I_k(s_k), x_k\right] p(x_k) \right\} p(s_k = s | s_{k-1} = s'). \qquad (2\text{–}32)\end{aligned}$$

Here, $I_l(s_l) = 0$ if $s_l \in \{E_0, S_0\}$, $I_l(s_l) = 1$ if $s_l \in \{E_1, S_1\}$ and $I_l(s_l) = -1$ if s_l is in any of the other $2K + 2$ states. For the first round of demodulation and decoding $p(x_k) = 0.5$.

Once the decoding is performed, this extrinsic information is fed back from the MAP decoder of the error correcting code.

The probability measure, $p\left(y_k^0, y_k^1 | I_{k-1}(s_{k-1}), I_k(s_k), x_k\right)$, is derived by integrating (2–2) over θ_1. For noncoherent demodulation, in which we assume that we have no knowledge of the channel phase of the desired user, we have

$$p\left(y_k^0, y_k^1 | I_{k-1}(s_{k-1}), I_k(s_k), x_k = l\right) = \exp\left[-\frac{1}{2\sigma^2}\left(|y_k^0 - A_2 g_k(\tau)|^2 + |y_k^1 - A_2 h_k(\tau)|^2 + |A_1|^2\right)\right] \times \mathrm{I}_0\left(\frac{|A_1|}{\sigma^2}|y_l - A_2 H_k(\tau, l)|\right), \quad (2\text{–}33)$$

where $\mathrm{I}_0(\cdot)$ is the modified Bessel function of the first kind.

For coherent demodulation, in which we assume that we have full knowledge of the channel phase of the desired user, the probability measure is given by

$$p\left(y_k^0, y_k^1 | I_{k-1}(s_{k-1}), I_k(s_k), x_k = l\right) = \exp\left[-\frac{1}{2\sigma^2}\left(|y_k^0 - A_2 g_k(\tau)|^2 + |y_k^1 - A_2 h_k(\tau)|^2 + |A_2|^2\right)\right] \times \exp\left(\frac{\mathrm{Re}\left\{A_1\left[(y_l - A_2 H_k(\tau, l)\right]^*\right\}}{\sigma^2}\right). \quad (2\text{–}34)$$

Finally, for the partially coherent demodulation, in which the phase of the desired user is modeled as a Tikhonov random variable with coherence parameter, α, evaluating (2–2) over (2–26) yields

$$p\left(y_k^0, y_k^1 | I_{k-1}(s_{k-1}), I_k(s_k), x_k = l\right) = \exp\left[-\frac{1}{2\sigma^2}\left(|y_k^0 - A_2 g_k(\tau)|^2 + |y_k^1 - A_2 h_k(\tau)|^2 + |A_2|^2\right)\right] \times \mathrm{I}_0\left(\frac{|A_1|}{\sigma^2}\sqrt{(\Upsilon_R)^2 + (\Upsilon_I)^2}\right), \quad (2\text{–}35)$$

where

$$\Upsilon_R = \mathrm{Re}\left[y_l - A_2 H_k(\tau, l)\right] + \frac{\sigma^2 \alpha}{|A_1|}\cos\theta_1$$

and

$$\Upsilon_I = \mathrm{Im}\left[y_l - A_2 H_k(\tau, l)\right] + \frac{\sigma^2 \alpha}{|A_1|}\sin\theta_1.$$

We present the a priori probabilities of the transition between the states, $p(s_k = s|s_{k-1} = s')$, derived in [22]. The results confirm the intuitive reasoning that the probabilities of symbols being in a particular type of hit are not equally likely and are a function of time, k. In other words, the leftmost bits in are dwell interval are much more likely to be interfered with by a hit that occurs on the left. For the different state transitions, the probabilities are given by

$$\begin{aligned}
p(s_k = S_j|s_{k-1} = S_i) &= \frac{1}{2}\left(1 - \frac{1}{N_D - k}\right), \qquad i, j \in 0, 1 \\
p(s_k = M_1|s_{k-1} = S_i) &= \frac{1}{N_D - k}, \qquad i \in 0, 1, \\
p(s_k = M_{i+1}|s_{k-1} = M_i) &= 1, \qquad i \in \{1, 2, ..., 2M\}, \\
p(s_k = E_X|s_{k-1} = M_{2M}) &= 1 - \frac{1}{F}, \\
p(s_k = E_i|s_{k-1} = M_{2M}) &= \frac{1}{2F}, \qquad i \in 0, 1,
\end{aligned}$$

$$\begin{aligned}
p(s_k = E_j|s_{k-1} = E_i) &= \frac{1}{2}, \qquad i, j \in 0, 1, \\
p(s_k = S_X|s_{k-1} = S_X) &= \begin{cases} 1 - \frac{1}{F(N_D+2M)-N_D-k}, & 0 \le k \le 2M \\ 1 - \frac{1}{F(N_D+2M)-(k-2M)}, & 2M \le k \le N_D \end{cases}, \\
p(s_{k+1} = E_i|s_{k-1} = S_X) &= \begin{cases} \frac{1}{2}\frac{1}{F(N_D+2M)-N_D-k}, & 0 \le k \le 2M \\ \frac{1}{2}\frac{1}{F(N_D+2M)-(k-2M)}, & 2M \le k \le N_D \end{cases} \qquad i \in 0, 1.
\end{aligned}$$

Given knowledge the branch metric , $\gamma(s', s)$, the forward and backward looking probabilities, $\alpha(s)$ and $\beta(s')$ are given [31] by

$$\alpha_{k+1}(s) = \sum_{s'} \alpha_k(s')\gamma_{k+1}(s', s),$$

and

$$\beta_{k-1}(s') = \sum_{s} \beta_k(s)\gamma_k(s', s).$$

The initial values of α and β are the probabilities that the trellis starts or ends at each initial or terminal state. These probabilities are given by

$$\begin{aligned}
\alpha_0(s = S_i) &= \frac{1}{2F}\left(\frac{N_D}{N_D + 2M}\right), \qquad i \in 0, 1, \\
\alpha_0(s = S_X) &= 1 - \frac{1}{F}\left(\frac{N_D}{N_D + 2M}\right), \\
\beta_{N_D}(s = S_i) &= 0, \qquad i, j \in 0, 1, \\
\beta_{N_D}(s = E_X) &= \frac{1}{F}\left(1 - \frac{1}{F}\right)\frac{N_D - 2M}{N_D + 2M}, \\
\beta_{N_D}(s = M_i) &= \frac{1}{F(N_D + 2M)}, \\
\beta_{N_D}(s = E_i) &= \frac{1}{2F}\left(\frac{N_D}{N_D + 2M}\right), \qquad i \in 0, 1, \text{and} \\
\beta_{N_D}(s = S_X) &= \frac{1}{F}\left(1 - \frac{1}{F}\right)\left(\frac{F(N_D + 2M) - (N_D - 2M))}{N_D + 2M}, \right).
\end{aligned}$$

Given these values, the joint a posteriori probability for consecutive interference symbols is given by

$$p(I_{k-1}, I_k|y) = C \sum_{U\{I_{k-1}, I_k\}} \alpha_{k-1}(s')\gamma_k(s', s)\beta_k(s), \tag{2–36}$$

where $I_k \in \{X, 0, 1\}$ and $U\{I_{k-1}, I_k\}$ is the set of all state transitions that have I_{k-1}, I_k as their branch outputs. Also, C is a probability normalization constant.

Given this information, we can generate the likelihood function of the received metric given the interference and the transmitted symbol as

$$p(y_k^0, y_k^1|x_k) = \sum_{I_{k-1}} \sum_{I_k} p(y_k^0, y_k^1|x_k, I_{k-1}, I_k) p(I_{k-1}, I_k), \tag{2–37}$$

where we have approximated $p(I_{k-1}, I_k)$ by $p(I_{k-1}, I_k|y)$.

The output of the soft demodulator is the log-likelihood ratio that combines this information with the extrinsic information provided by the decoder. The log-likelihood ratio is calculated as

$$LLR(x_k) = \text{log}\frac{p(y_k^0, y_k^1|x_k = 0)}{p(y_k^0, y_k^1|x_k = 1)} + \text{log}\frac{p(x_k = 0)}{p(x_k = 1)}. \tag{2–38}$$

Also, we present results, motivated in **??**, where we replace the noise variance in (2–33), (2–34) and (2–35) with the estimated channel variance.

2.5 Performance Results

We evaluated the performance of our receiver using computer simulations. 1000 encoded bits are interleaved and transmitted over 10 frequency bands. Information bits are encoded using a rate $1/2$ convolutional code of constraint length 7 of maximum free distance and interleaved using a pseudo-random channel interleaver before transmission. The channel parameters A_1 and A_2 are modeled as complex Gaussian random variables that are constant within a dwell interval and independent among dwell intervals. The time offset between users, τ, is uniformly distributed on $(0, T]$. We assume that all the parameters other than the desired user's timing are unknown at the receiver, and we compare the performance of a system employing partially coherent demodulation to ones utilizing coherent and noncoherent demodulation.

We first consider a system in which each dwell interval experiences interference from at most one user. For this scenario, we consider a simple system containing two users contending over ten frequency bands. Fig. 2-5 shows a comparison in the performance of partially coherent demodulation and the more traditional coherent and

non-coherent approaches. We see from the figure that partially coherent demodulation performs as well or better than both of the other demodulation schemes for all values of E_b/N_0. We also see that at low E_b/N_0, our approach is able to adapt and get performance that closely matches that provided by fully coherent demodulation, but as the channel becomes less noisy, we see a substantial drop in the error floor compared to coherent demodulation (about an order of magnitude).

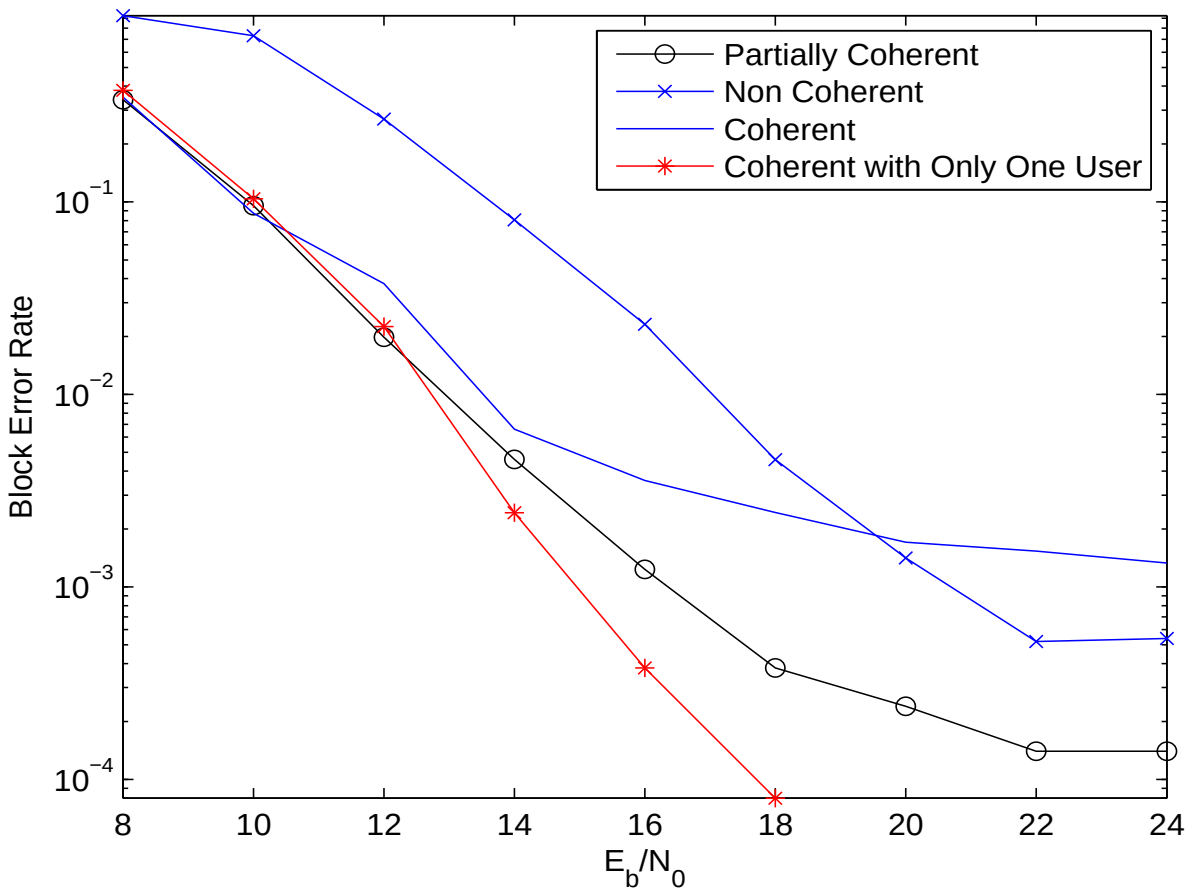

Figure 2-5. Block error rate vs. E_b/N_0 for two users contending on ten frequency bands in a Rayleigh channel with SIR= 0dB.

Next, we consider how the strength of the interference affects performance. We consider a $2-$user system with ten frequency bands available for transmission and a fixed $E_b/N_0 = 20$ dB. Fig. 2-6 presents the block error rate as a function of

the signal-to-interference ratio. We see that we get about a 3 dB gain across all SIR's compared to the noncoherent case and at least 2 dB improvement for the coherent case. We also observe the presence of an error floor that severely affects the performance when using coherent demodulation in this environment.

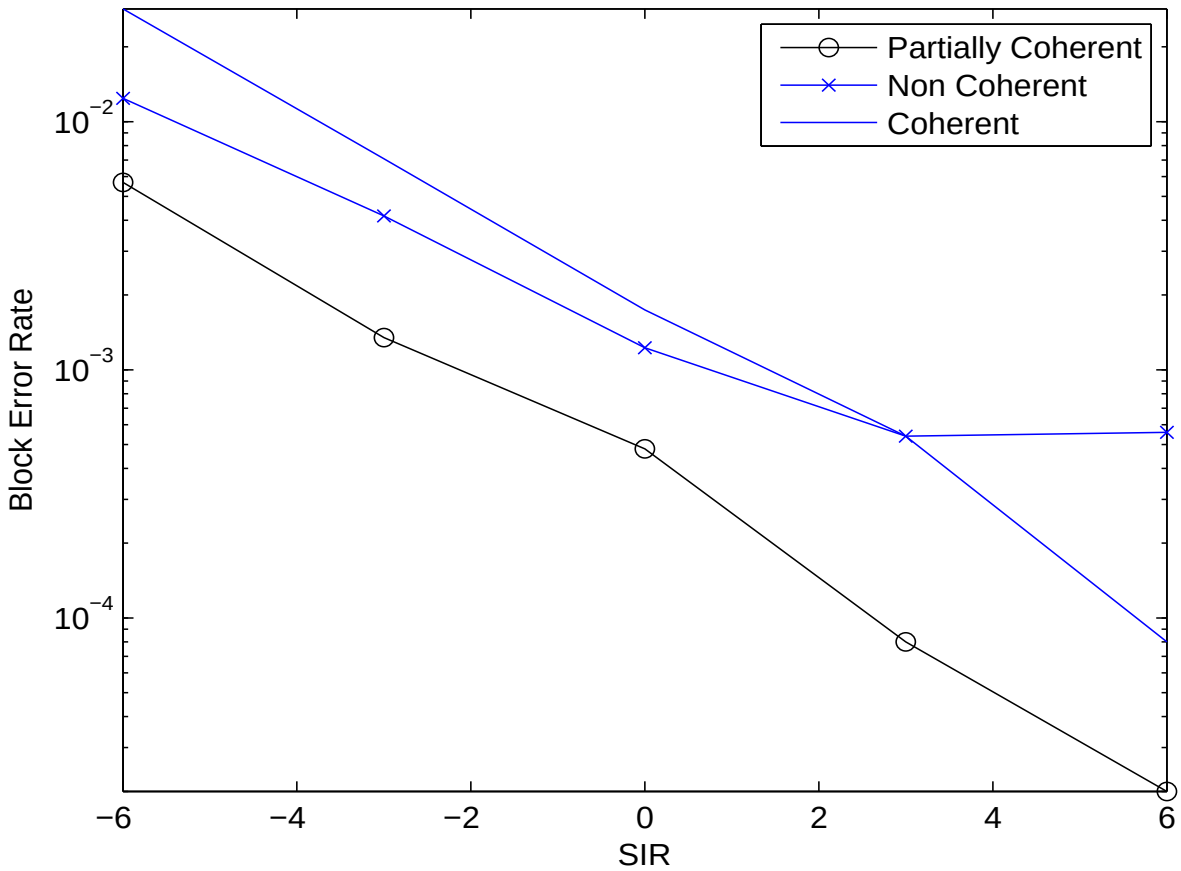

Figure 2-6. Block error rate vs. SIR for two users contending on ten frequency bands in a Rayleigh channel with $E_b/N_0 = 20$ dB.

Fig. 2-7 shows the block error rates as a function of E_b/N_0 at selected numbers of iterations. There is little performance to be gained after 12 iterations. We also present the evolution of α across iterations in Fig. 2-8. We see evidence of improvement in the channel estimate as the iteration progresses. In Fig. 2-9 and Fig. 2-10, we consider

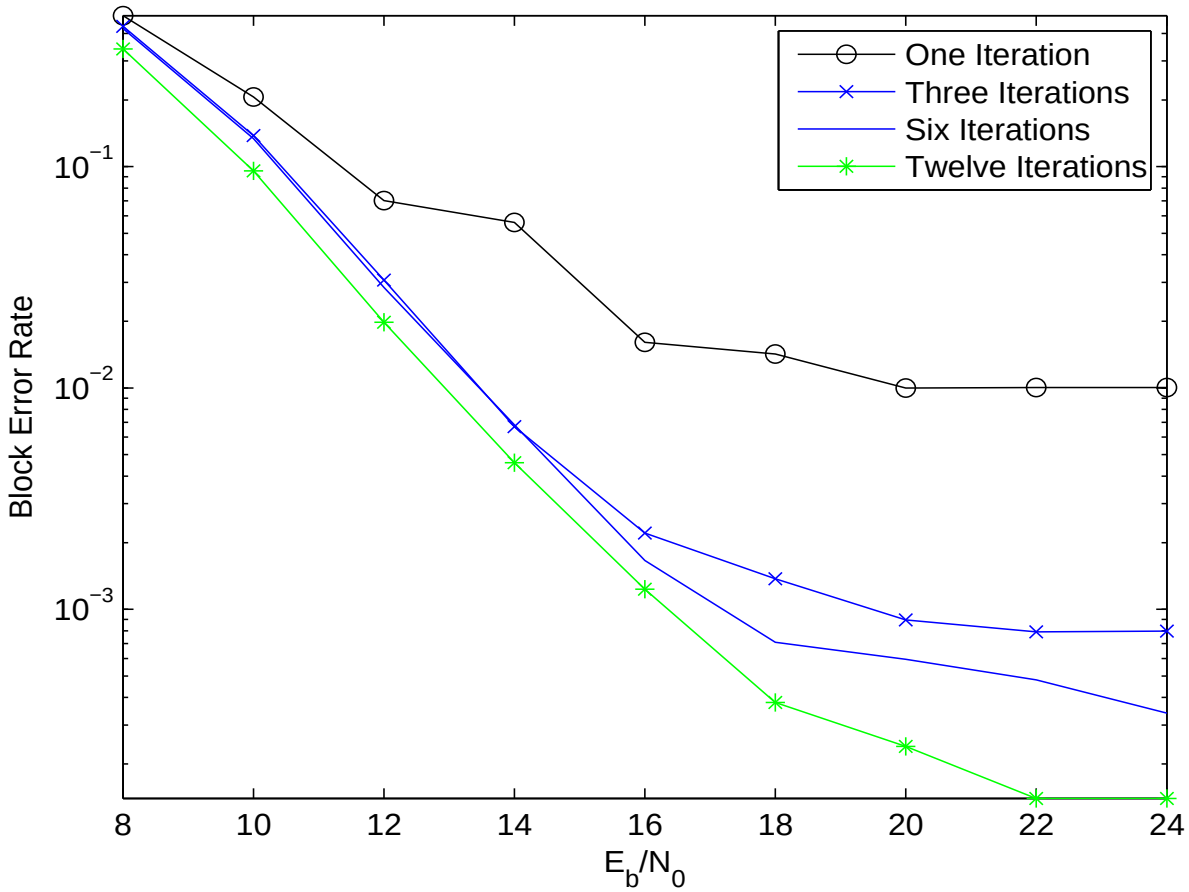

Figure 2-7. Performance over selected number of iterations, SIR=0 dB.

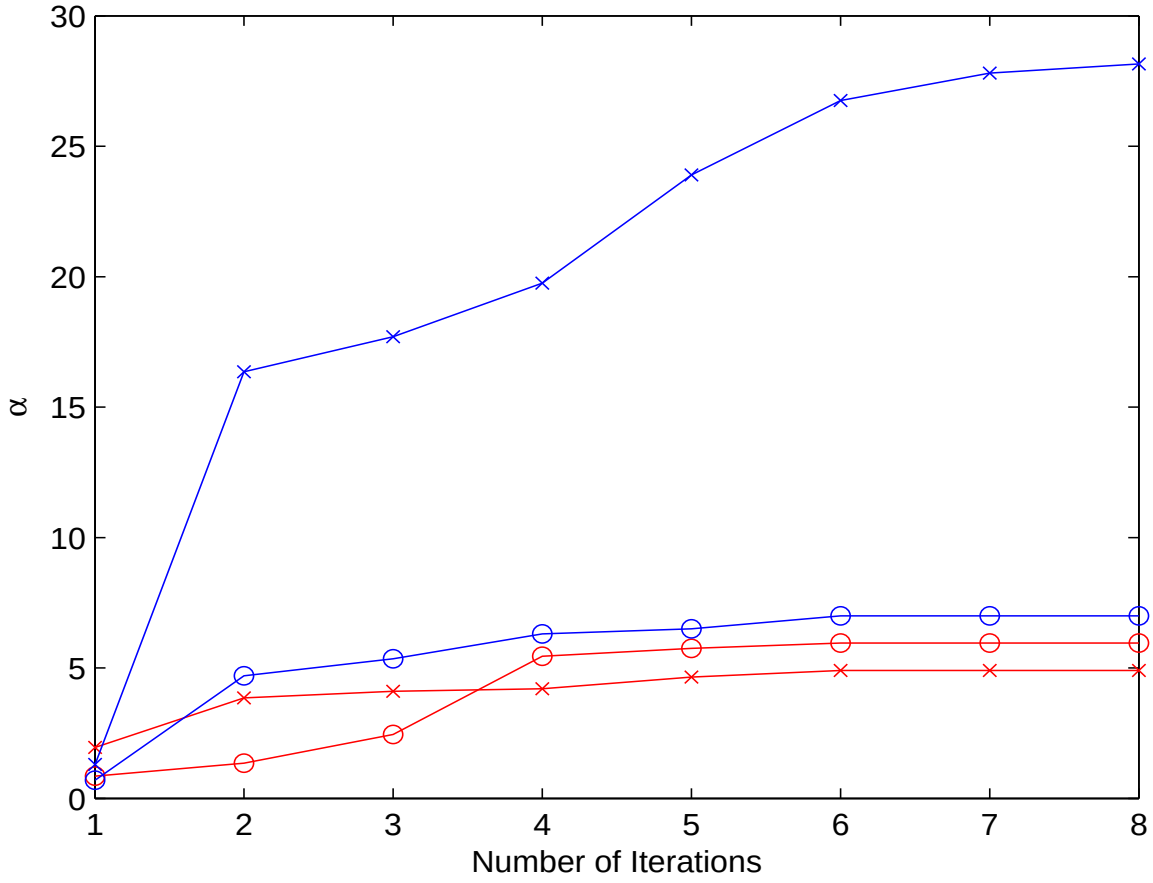

Figure 2-8. Evolution of α across iterations for selected dwell intervals.

a more realistic system in which multiple users contend over 100 frequency bands. Fig. 2-9 presents the block error rate as a function of the number of users. We can see that the performance curves for coherent and noncoherent demodulation are very similar. However, for a system using partially coherent demodulation in this scenario, we get about a 40% improvement in the number of users that can be supported at a target error rate of 10^{-2}. For Fig. 2-10, we consider a system operation at SIR=0 dB

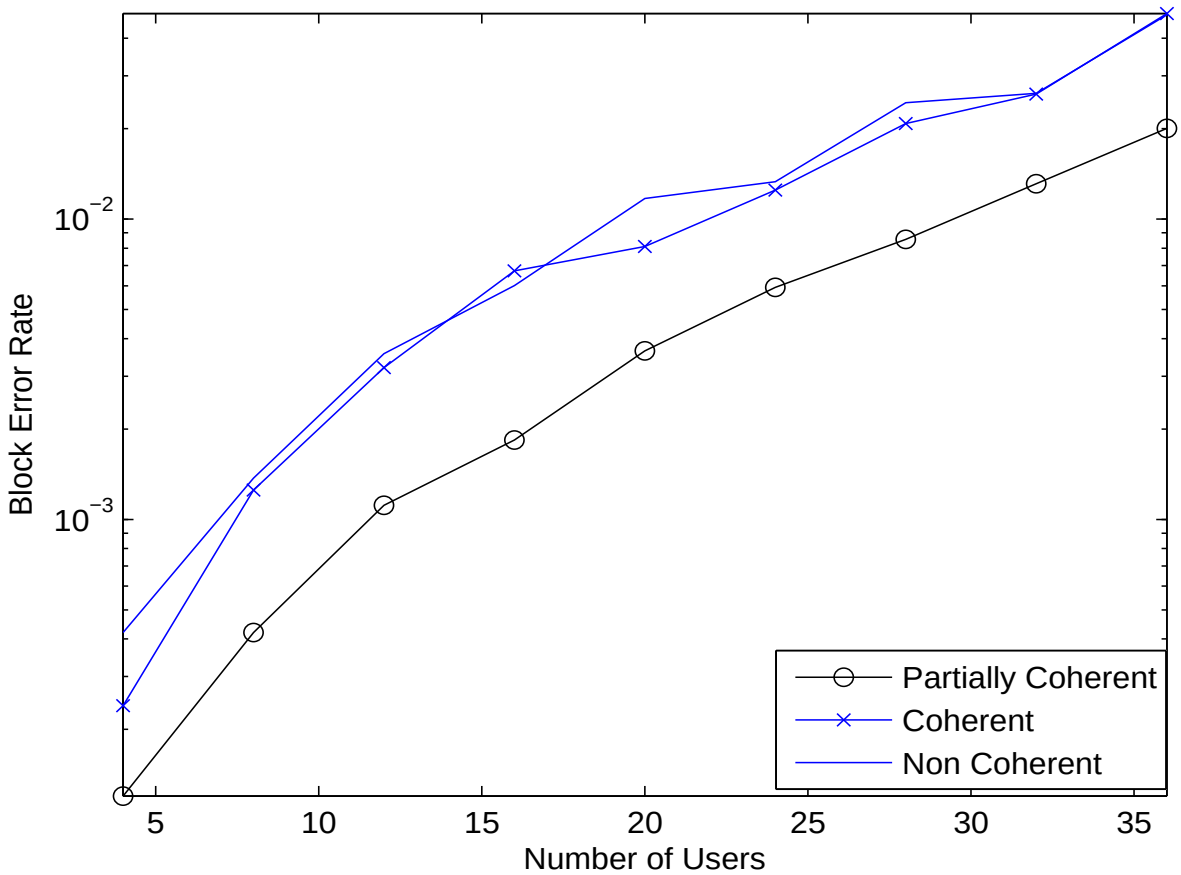

Figure 2-9. Block error rate vs. number of users, $E_b/N_0 = 24$ dB, SIR=0 dB.

and investigate the maximum number of users that can be supported at each E_b/N_0 at a target error rate of 10^{-2} . We see that partially coherent demodulation outperforms the better of the comparison cases across all E_b/N_0 by supporting up to 44% more users.

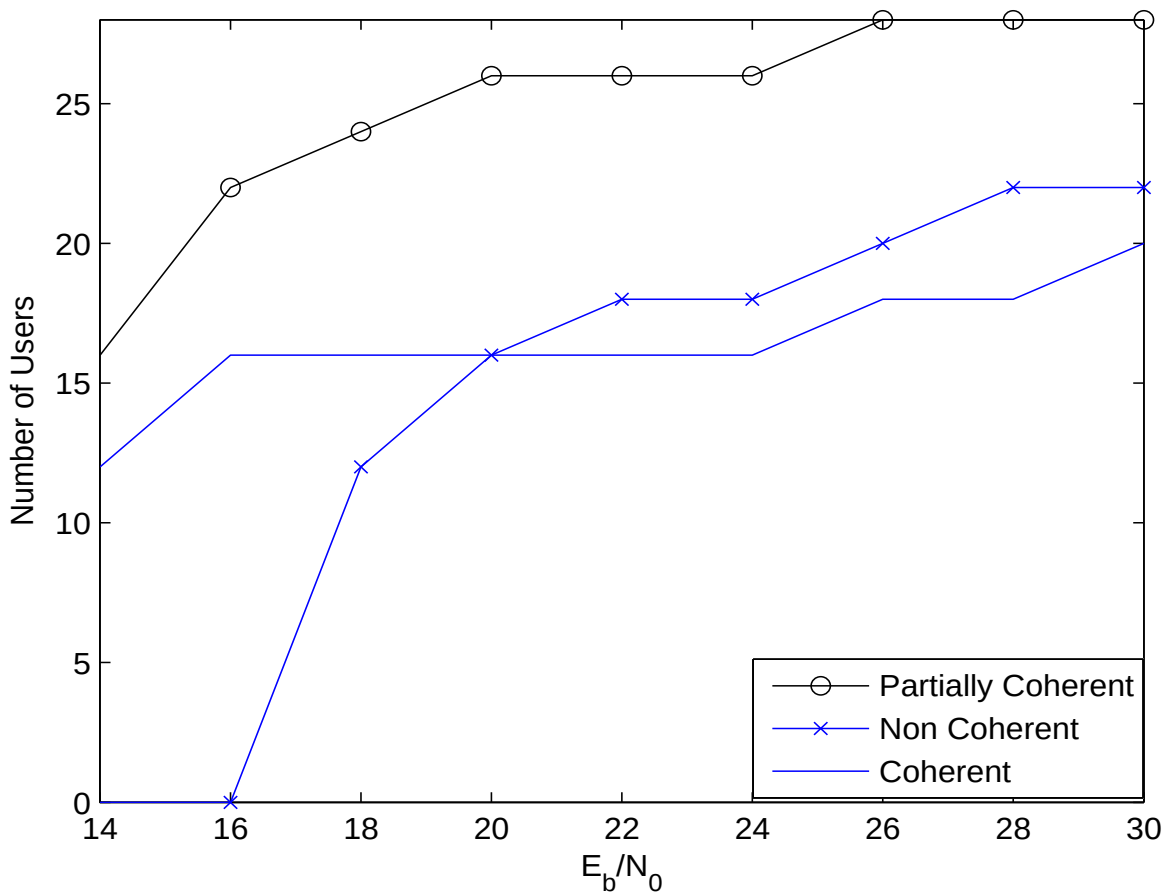

Figure 2-10. Maximum number of users that can be supported for a target error rate of 10^{-2} in a system in which users contend over 100 frequency bands at SIR= 0 dB

The results for the case where the noise variance is replaced by the channel variance is shown in Fig. 2-11 and Fig. 2-12 We see that this approach provides superior interference mitigation capability across all Eb/N_0. We also see in Fig. 2-12 that far more users are supported when compared to the case of no interference mitigation. In particular, we see an improvement of more than 100% in the number of users that can be supported at a target error rate of 10^{-2} for the coherent and partially coherent cases. However, we also see that partially coherent does not provide a significant performance gain over coherent demodulation because in the coherent demodulator, the errors in the reference phase result in additional noise that can be treated as approximately Gaussian.

2.6 Summary

In this section, we have used partially coherent demodulation to improve the performance of an interference mitigating receiver. We quantified our level of confidence in the estimate of the parameters of the desired user and we have used this new quantity to aid in demodulation. We have shown that this iterative partially coherent demodulation approach provides more robustness to interference. We have also shown substantial gains in the multiple-access capability of the system. Finally, we have shown that additional performance gains can be achieved when the thermal noise variance is replaced by the estimated channel variance during demodulation.

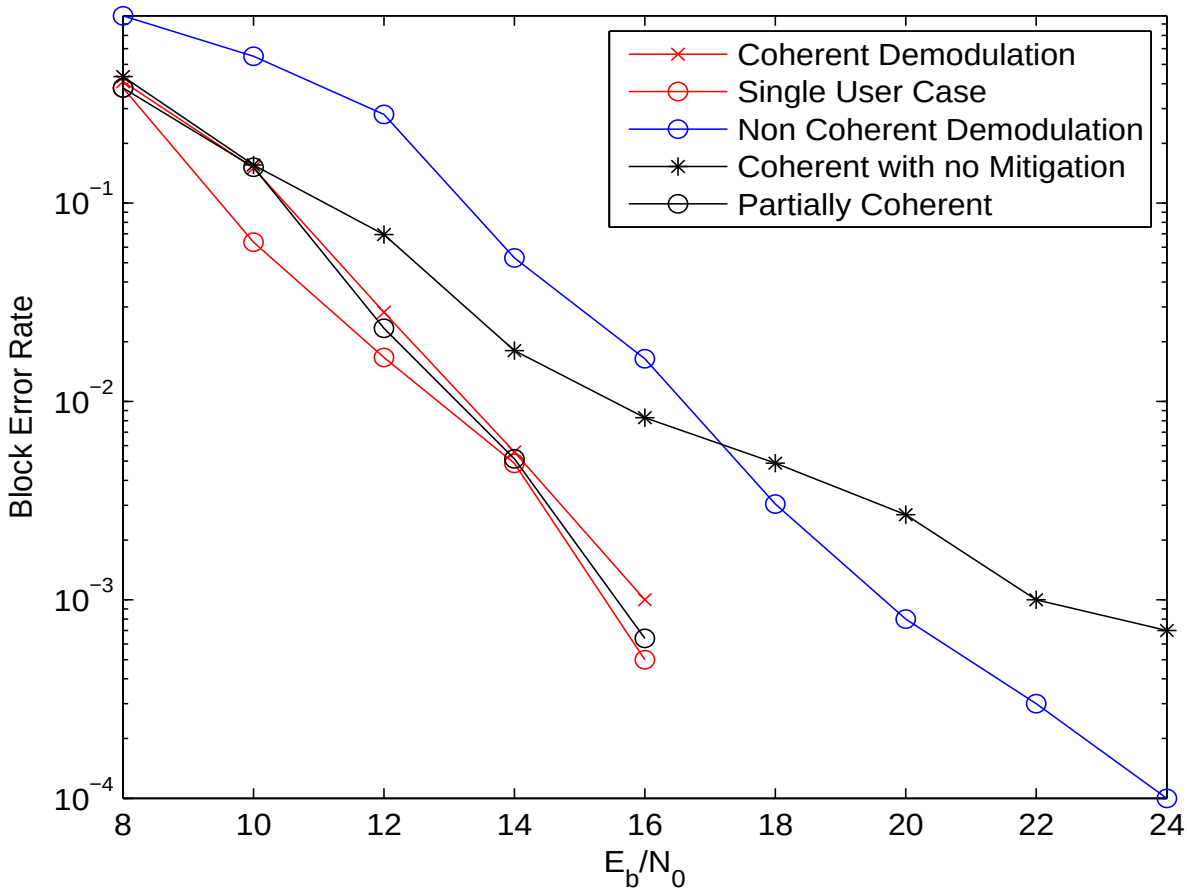

Figure 2-11. Block error rate vs. E_b/N_0 for two users contending on ten frequency bands in a Rayleigh channel with SIR= 0dB: Channel variance estimation case.

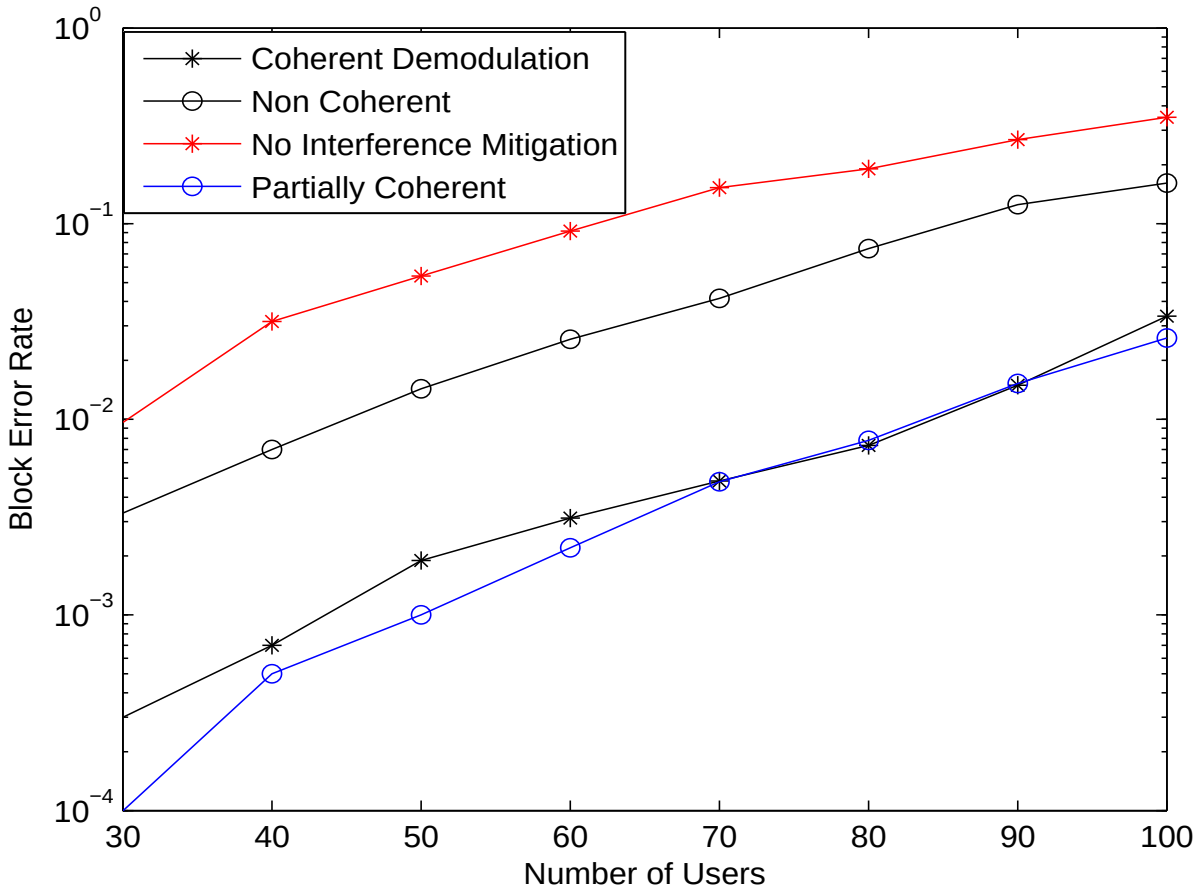

Figure 2-12. Block error rate vs. number of users, $E_b/N_0 = 24$dB, SIR=0dB: channel variance estimation case.

CHAPTER 3
MULTIPLE-ACCESS INTERFERENCE MITIGATION AND ITERATIVE DEMODULATION OF CPFSK IN ASYNCHRONOUS SLOW FHSS SYSTEMS

3.1 Introduction of Multiple-Access Interference Mitigation and Iterative Demodulation of CPFSK in Asynchronous Slow FHSS Systems

The issue of MAI mitigation in CPFSK-modulated FHSS system is a more challenging one because CPFSK is not a memoryless modulation scheme. The traditional approach to dealing with MAI in this system involves treating the interference as noise. This approach has been shown to work well if the signal-to-interference ratio is high [27, 28]. However, this approach does not work well for low signal-to-interference ratio. This is because it disregards the fact that for the most likely scenario of one strong interferer in a dwell interval, there is a structure to the interference contained in that interval.

In this chapter, we exploit the structure of the interference with the goal of designing a more robust system. We show performance gains in terms of the block error rate and multi-access capability of the system. The rest of the chapter is arranged as follows. In Section 3.2, we introduce the system model and derive the channel likelihood for demodulation of CPFSK. In Section 3.3, we describe how the parameters of the channel is estimated, and in Section 3.4, we give an explanation on how demodulation is performed. Performance results from simulations are presented in Section 3.5, and the chapter is concluded in Section 3.6.

3.2 System Model

The system model considered in this chapter is illustrated in Fig. 3-1. We consider a FHSS system with multiple users transmitting simultaneously. The transmitters are identical, but the frequency hopping patterns vary from one user to the other. Data is convolutionally coded, and the symbols at the output of the encoder are interleaved and packed into a frame of fixed length. These bits are then divided into segment of D data bits and modulated using CPFSK. In each dwell interval, the D data bits are transmitted

along with P pilot symbols and N null symbols on each side of the data symbols, as shown in Fig. 3-2. During the null symbols, no transmission occurs, which allows the receiver to detect and estimate the presence of MAI.

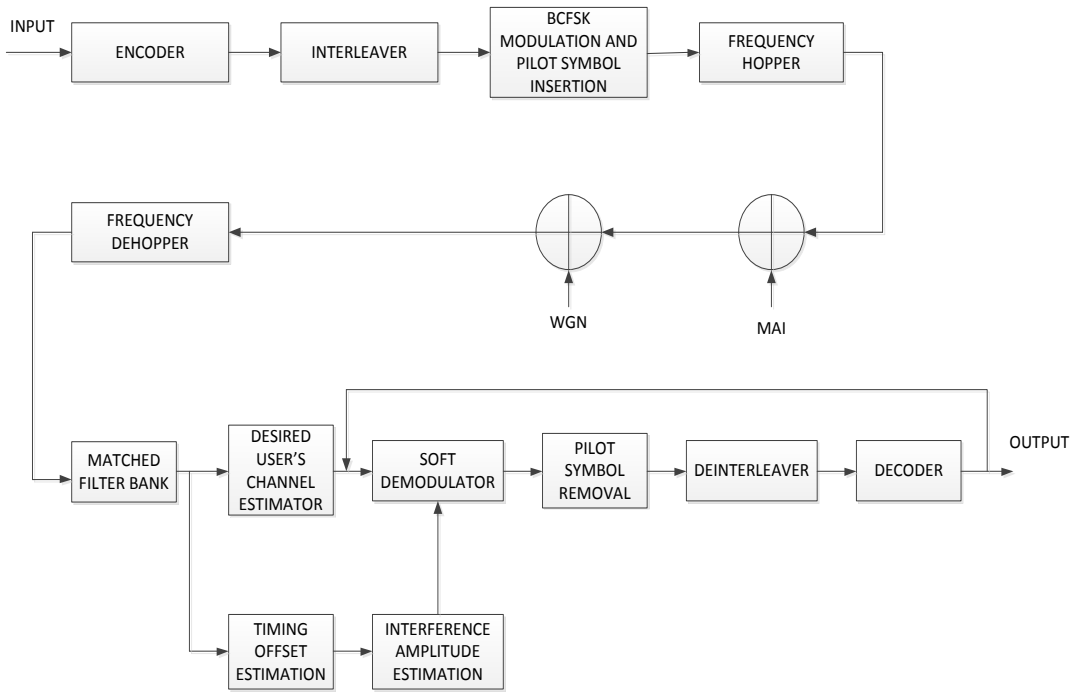

Figure 3-1. System model.

Let $\boldsymbol{q}$ denote the input sequence to the modulator for a particular dwell interval. For M-ary CPFSK, the entries of $\boldsymbol{q}$ are chosen from the alphabet set $Q = \{0, 1, ..., M-1\}$. For the ith symbol in $\boldsymbol{q}$, the modulated signal $x_i(t)$ is chosen as the $q_i(th)$ signal in the set $\mathcal{S} = \{s_k(t), k = 0, 1, ..., M-1\}$, where

$$s_k(t) = \frac{1}{\sqrt{T}} \exp \frac{jh\pi(2k-(M-1))t}{T_s}, t \in [0, T_s).$$

Here h is the modulation index and T_s is the symbol duration. In order to maintain continuous phase transitions between consecutive symbols, this phase is accumulated as

$$\phi_{i+1} = \phi_i + (2q_i - (M-1))\pi h.$$

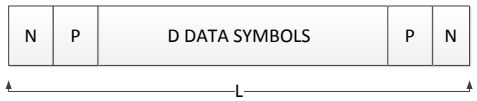

Figure 3-2. Structure of a dwell interval. P and N denote sets of pilot and null symbols, respectively.

For simplicity, in this chapter, we focus on the binary case ($M = 2$), although our techniques can be applied for other M.

The resulting CPFSK symbols are modulated onto a carrier according to the slow frequency-hopping scheme. The channel is divided into F frequency bands. A pseudo-random hopping sequence is used to choose a carrier frequency for each dwell interval. All the symbols in a particular dwell interval are then transmitted at the same carrier frequency. Because the hopping patterns of different users are not orthogonal, MAI occurs when multiple users transmit at the same time on the same carrier frequency. The signals arrive at the receiver with random amplitudes and phases. The channel is a slow frequency-selective Rayleigh fading channel. We model this using block fading in which the amplitude and phase are constant over each dwell interval but vary from one dwell interval to another.

At the receiver, the received signal is dehopped and passed through a bank of M pairs of matched filter with one pair matched to the in-phase and quadrature components of each frequency tone. We assume that the receiver can achieve perfect timing for the desired signal[1] . However, any interfering signals are asynchronous to the desired signal. As in the previous chapter, we design the interference mitigation scheme based on the presence of one strong interfering user, and the receiver must detect and obtain timing information for the interference in any dwell interval for which there is MAI.

[1] If it cannot obtain good timing information for the desired signal, then it will have no possibility of recovering it.

Consider a desired symbol that is received in the presence of an interfering signal for which the symbol boundaries are τ seconds delayed with respect to the symbol boundaries of the desired signal, i.e $0 \leq \tau \leq T_s$. After it is matched filtered and sampled, the received signal can be written in vector form as

$$\boldsymbol{y} = A_1 \boldsymbol{x} e^{j\phi} + A_2 \boldsymbol{I} \boldsymbol{\psi} + \boldsymbol{n}, \tag{3–1}$$

where $A_1 = a_1 e^{j\theta_1}$ and $A_2 = a_2 e^{j\theta_2}$ are the complex channel gains of the desired and interfering user, respectively. Here, $\boldsymbol{I}$ is an M by 2 matrix whose rows, $\boldsymbol{I_k}$, model the effect of interference in the matched filter and $\boldsymbol{\psi}$ models the phases of the interference symbols. Since the interference is asynchronous, the output of the matched filters are associated with two consecutive interfering symbols. Each element of $\boldsymbol{y}$ can be represented as

$$y_k = A_1 x_k e^{j\phi} + A_2 \boldsymbol{I_k} \boldsymbol{\psi} + n_k,$$

where

$$\begin{aligned}
x_k &= \int_0^{T_s} x(t) s_k^*(t) dt, \\
n_k &= \int_0^{T_s} n(t) s_k^*(t) dt, \\
\boldsymbol{I_k} &= \left[\int_0^{\tau} s_m(t - \tau + T_s) s_k^*(t) dt, \int_{\tau}^{T_s} s_n(t - \tau) s_k^*(t) dt \right], \\
\boldsymbol{\psi} &= \left[e^{j\psi_{i-1}}, e^{j\psi_i} \right]',
\end{aligned}$$

and $(s_m(t), s_n(t)) \in \mathcal{S}, \forall (m, n) \in \{0, 1\}$. The noise vector is Gaussian with a covariance matrix $\boldsymbol{R} = E[\boldsymbol{n}\boldsymbol{n}^H]$ whose entries are given by

$$r_{k,i} = \mathrm{Sinc}(\pi(i - k)h) e^{j\pi(i-k)h},$$

where

$$\mathrm{Sinc}(x) = \begin{cases} 1 & \text{if } x = 0, \\ \frac{\sin(x)}{x} & \text{otherwise.} \end{cases}$$

It then follows that the matrix $\boldsymbol{I}$ is of the form

$$\begin{bmatrix} I_{1,1}, I_{1,2} \\ I_{2,1}, I_{2,2} \end{bmatrix},$$

since there are at most two interference symbols in a desired symbol interval. Consider the output of the matched filter for $s_k(t)$ in the presence of consecutive interference symbols $s_m(t)$ and $s_n(t)$. Then the interference terms are given by

$$I_{k,1} = \begin{cases} 0, & \text{if } s_m(t) = 0 \\ \frac{\tau}{T_s} \exp - \frac{ih(-1+2k)\pi(T_s+\tau)}{T_s}, & \text{if } m = k \\ \frac{i\left(\exp\left(\frac{ih(-1+2m)\pi(T_s-\tau)}{T_s}\right) - \exp\left(\frac{ih\pi((-1+2m)T_s+\tau-2k\tau)}{T_s}\right)\right)}{2h(-k+m)\pi}, & \text{if } m \neq k \end{cases} \quad (3\text{–}2)$$

and

$$I_{k,2} = \begin{cases} 0, & \text{if } s_m(t) = 0 \\ \left(1 - \frac{\tau}{T_s}\right) \exp\left(\frac{ih(1-2k)\pi\tau}{T_s}\right), & \text{if } n = k \\ -\frac{i\left(\exp\left(-\frac{ih(-1+2k)\pi\tau}{T_s}\right) - \exp\left(-\frac{ih\pi(2kT_s-2nT_s-\tau+2n\tau)}{T_s}\right)\right)}{2h(k-n)\pi}, & \text{if } n \neq k. \end{cases} \quad (3\text{–}3)$$

To simplify the notation, we define the channel parameter vector $\boldsymbol{\Upsilon} = \{a_1, a_2, \theta_1, \theta_2, \tau\}$. The probability density function of $\boldsymbol{y}$ given $\boldsymbol{x}$, $\boldsymbol{I}$, and $\boldsymbol{\Upsilon}$ is

$$p(\boldsymbol{y}|\boldsymbol{x}, \boldsymbol{I}, \boldsymbol{\Upsilon}) = \frac{1}{\pi^M \det(\boldsymbol{R})} \exp\left\{-(\boldsymbol{y} - A_1\boldsymbol{x}e^{j\phi} - A_2\boldsymbol{I}\boldsymbol{\psi})^H \right.$$
$$\left. \times \boldsymbol{R}^{-1}(\boldsymbol{y} - A_1\boldsymbol{x}e^{j\phi} + A_2\boldsymbol{I}\boldsymbol{\psi}.\right\} \quad (3\text{–}4)$$

The exponential term in the density function can be written as

$$-(\boldsymbol{y}^H \boldsymbol{R_n}^{-1}\boldsymbol{y} - 2\,\mathrm{Re}(A_1 e^{j\phi}\boldsymbol{y}\boldsymbol{R_n}^{-1}\boldsymbol{x}) - 2\,\mathrm{Re}(A_2\boldsymbol{y}^H\boldsymbol{R_n}^{-1}\boldsymbol{I}\boldsymbol{\psi}) + |A_1|^2\boldsymbol{x}^H\boldsymbol{R_n}^{-1}\boldsymbol{x} + 2\,\mathrm{Re}(A_1^* A_2 e^{-j\phi}\boldsymbol{x}^H\boldsymbol{R_n}^{-1}\boldsymbol{I}\boldsymbol{\psi}) + |A_2|^2\boldsymbol{\psi}^H\boldsymbol{I}^H\boldsymbol{R_n}^{-1}\boldsymbol{I}\boldsymbol{\psi}. \quad (3\text{–}5)$$

Define $\boldsymbol{K} = \frac{1}{2\sigma^2}\boldsymbol{R_n}$. When $x(t) = s_v(t)$, $\boldsymbol{x}$ is the vth column of $\boldsymbol{K}$. Then (3–5) becomes

$$\frac{-\boldsymbol{y}^H\boldsymbol{K}^{-1}\boldsymbol{y} + 2\,\mathrm{Re}(A_2\boldsymbol{y}^H\boldsymbol{K}^{-1}\boldsymbol{I}\boldsymbol{\psi})}{2\sigma^2} - \frac{|A_1|^2 - |A_2|^2\boldsymbol{\psi}^H\boldsymbol{I}^H\boldsymbol{K}^{-1}\boldsymbol{I}\boldsymbol{\psi}}{2\sigma^2} + \frac{2\,\mathrm{Re}(A_1 e^{j\phi}y_v) - 2\,\mathrm{Re}(A_1^* A_2 e^{-j\phi}(\boldsymbol{I}\boldsymbol{\psi})_v)}{2\sigma^2}. \quad (3\text{–}6)$$

Here, $(\boldsymbol{I}\boldsymbol{\psi})_v$ is defined as the vth element of the product of $\boldsymbol{I}$ and $\boldsymbol{\psi}$. Define $\hat{y_v} = \angle y_v$ and $\hat{I_v} = \angle I_v$.

The use of pilot symbols whose induced phases are known *a priori* at the receiver allows for channel estimation of the desired user at the receiver. So, given estimates of the channel parameters of the desired user, we can integrate (3–6) over the uniform random variable θ_2 to yield

$$\exp\left\{\frac{-\boldsymbol{y}^H\boldsymbol{K}^{-1}\boldsymbol{y} - |A_1|^2 + 2\,\mathrm{Re}(A_1 e^{j\phi}y_v)}{2\sigma^2} - \frac{|A_2|^2\boldsymbol{\psi}^H\boldsymbol{I}^H\boldsymbol{K}^{-1}\boldsymbol{I}\boldsymbol{\psi}}{2\sigma^2}\right\} I_0\left(\frac{|A_2|}{\sigma^2}\sqrt{\Omega_r^2 + \Omega_i^2}\right) \quad (3\text{–}7)$$

where

$$\Omega_r = \mathrm{Re}(\boldsymbol{y}^H\boldsymbol{K}\boldsymbol{I}\boldsymbol{\psi}) - \mathrm{Re}(A_1^* e^{-j\phi}(\boldsymbol{I}\boldsymbol{\psi})_v)),$$

$$\Omega_i = (\mathrm{Im}(\boldsymbol{y}^H\boldsymbol{K}\boldsymbol{I}\boldsymbol{\psi}) - \mathrm{Im}(A_1^* e^{-j\phi}(\boldsymbol{I}\boldsymbol{\psi})_v),$$

and $I_0(\cdot)$ is the zeroth order modified Bessel function of the first kind.

3.3 Parameter Estimation

The parameters of the desired and interfering users must be estimated before interference mitigation can be performed using the soft demodulation scheme described in Section 3.4. The user's channel parameters are estimated using the pilot symbols at the beginning and end of each dwell interval. The reliability of the estimates from each set of pilot symbols is determined and used in deciding which set to use for the desired user's channel estimate and which set of null symbols to use in estimating the parameters of the interfering user. Next, we compute the relative timing offset of the interfering user by using the null symbols in dwell intervals containing interference. Once we have an estimate of the symbol offset, we use this estimate to calculate the magnitude of the interference in each dwell interval.

3.3.1 Channel Estimator (Desired User)

To maintain the continuous phase requirement of CPFSK, a group of P pilot symbols are inserted after the M null symbols and another group is inserted after the data block. We estimate the parameters of the desired user using the pilot symbols. In particular, we perform this estimate assuming that at least one of the two sets of pilot symbols have not been interfered with. Since the pilot symbols are positioned on both sides of the data block, we generate two estimates of A_1 and choose the estimate that provides the best reliability, as suggested by a coherence parameter. For each pilot symbol, the local estimate for the channel is given by

$$\hat{A}_{1k} = \boldsymbol{w}_k^T \boldsymbol{y}_k e^{-j\phi_k}, \tag{3–8}$$

where k is a pilot symbol position that is a member of a contiguous group of P pilot symbols that flank the data block on the left or right and $(\cdot)^T$ denotes the transpose

operation. The vector $\boldsymbol{w}_k$ is defined as

$$w_{ki} = \begin{cases} 1 & \text{if } x_{ki} = 1, \\ 0 & \text{if otherwise,} \end{cases} \tag{3–9}$$

where y_{ki} and w_{ki} are the ith elements of vectors $\boldsymbol{y}_k$ and $\boldsymbol{w}_k$ respectively. It then follows that

$$\hat{A}_1 = \frac{1}{P} \sum_{k=0}^{P} \hat{A}_{1k}, \tag{3–10}$$

for each group of pilot symbols.

It was empirically determined that if the estimate of α from both sides is greater than 10, the estimates can be combined in order to provide more data points for estimation. In the case where only one side is deemed reliable, i.e its coherence parameter is greater than 10, only that side is used in estimation. For the case where both sides are deemed unreliable, we choose the estimate from the side with a higher coherence parameter.

3.3.2 Timing Offset Estimator (Interfering User)

At the null positions, the amplitude of the desired user is zero. It then follows from (3–7) that the probability of $\boldsymbol{y}$ at these symbol positions is given by

$$p(\boldsymbol{y}|\boldsymbol{x}, \boldsymbol{I}, \boldsymbol{\Upsilon} \setminus \{\theta_2, \theta_1, a_1\}) \propto \exp \frac{-\boldsymbol{y}^H \boldsymbol{K}^{-1} \boldsymbol{y} - |A_2|^2 \boldsymbol{\psi}^H \boldsymbol{I}^H \boldsymbol{K}^{-1} \boldsymbol{I} \boldsymbol{\psi}}{2\sigma^2} \times I_0 \left(\frac{|A_2|}{\sigma^2} \left| (\boldsymbol{y}^H \boldsymbol{K} \boldsymbol{I} \boldsymbol{\psi} \right| \right), \tag{3–11}$$

where $\setminus$ represents the set-minus operation.

From (3–2) and (3–3), we can re-write the interference matrix $\boldsymbol{I}$ to be a function of the offset, τ/T_s, instead of τ. The maximum-likelihood (ML) estimate cannot be derived in analytical form from (3–11), so we use a brute-force search by quantizing the search space. We assume that the offset is from a finite set whose entries are

δ-spaced between 0 and 1. We then evaluate (3–11) for each offset value in the set across consecutive null symbols using the Viterbi algorithm. The initial estimate of $|A_2|$ used in (3–11) is calculated by taking the sum of the magnitudes of the matched filter outputs at each null position and taking the average across all the null positions.

The offset value that provides the most probable interference sequence is chosen along with its corresponding interference parameters. At this point, we have both an estimate for the offset and the interference matrix at each symbol position.

3.3.3 Interfering Channel Estimation

From (3–1), the output of the matched filter at the null positions is given by

$$\boldsymbol{y} = A_2 \boldsymbol{I} \boldsymbol{\psi} + \boldsymbol{n} \tag{3–12}$$

The initial estimate of $|A_2|$ used in the first iteration of the offset estimation is derived by taking the average of the magnitudes of $\boldsymbol{y}$ over all its elements and over both left and right clusters of null symbols. We determine whether to use the left or right estimates based on the coherence parameter. In other words, interference parameters are estimated using only the side with **low** reliability.

For subsequent iterations, it follows that the local estimate of the amplitude of the interfering user at each null symbol position can be written as

$$\left| \frac{(\boldsymbol{I}\boldsymbol{\psi})^* \boldsymbol{y}}{(\boldsymbol{I}\boldsymbol{\psi})^* \boldsymbol{I}\boldsymbol{\psi}} \right| = \left| \hat{A}_2 \right|_n \tag{3–13}$$

We derive an estimate for $|A_2|$ by averaging the local estimates. This new value is then fed back into the offset estimation block until it converges.

3.4 Soft Demodulator

Initial demodulation is performed in the traditional way, where we treat the interference as noise. However, if we fail to decode the frame after a set number of iterations, we apply soft demodulation to aid in detecting the desired signal in the presence of the MAI. Each dwell interval is demodulated using a 20-state trellis,

where each state is characterized by an ordered pair of a symbol phase and a right edge interfering phase of the desired symbol. If we assume that the set of symbol phases is given by $C = \{0, 0.5\pi, \pi, 1.5\pi\}$ and the set of interfering phases is given by $D = \{X, 0, 0.5\pi, \pi, 1.5\pi\}$, then, the Cartesian product, $C \times D$, corresponds to all possible states. The component $X \in D$ is used to denote that no interference is present.

The input to the trellis is a 2-tuple that consists of an ordered pair from the Cartesian product of $R = \{0, 1\}$ and $S = \{X, 0, 1\}$, where R is the set of all possible values for the desired symbol and S is the set of all possible interfering symbol values. The next state of the trellis is derived by calculating its state attributes. In particular, the phase continuity property of CPFSK is enforced so that,

$$\phi_{k+1} = \phi_k + (2r - (M-1))\pi h, r \in R,$$

where ϕ_k is the phase of the desired user at the current state. The same formula is applied to finding the next interference phase. The state with these two attributes is chosen as the next state.Fig. 3-3 gives a pictorial representation if the trellis and the state transitions are shown for a selected state. The branch metric for the transition is calculated by using (3–7) and the extrinsic information from the decoder. It is given by

$$LL(v_{k+1}|v_k) = \log\left[p(\boldsymbol{y}|\boldsymbol{x}, \boldsymbol{I}, \boldsymbol{\Upsilon} - \{\theta_2\})\right] + \log\left[p(x_k = r)\right]. \tag{3–14}$$

For the case where the desired user's channel estimate is deemed unreliable and there are enough dwell intervals with reliable estimates, the symbols within the unreliable dwell interval are erased before being sent to the decoder.

3.5 Simulation Results

The performance of the scheme provided in this chapter is examined and compared to the case where the receiver does not try to mitigate the effect of the interference. In one of the comparison cases, we use perfect estimates of the parameters of the desired user but use computed estimates for the other case. We provide results for a

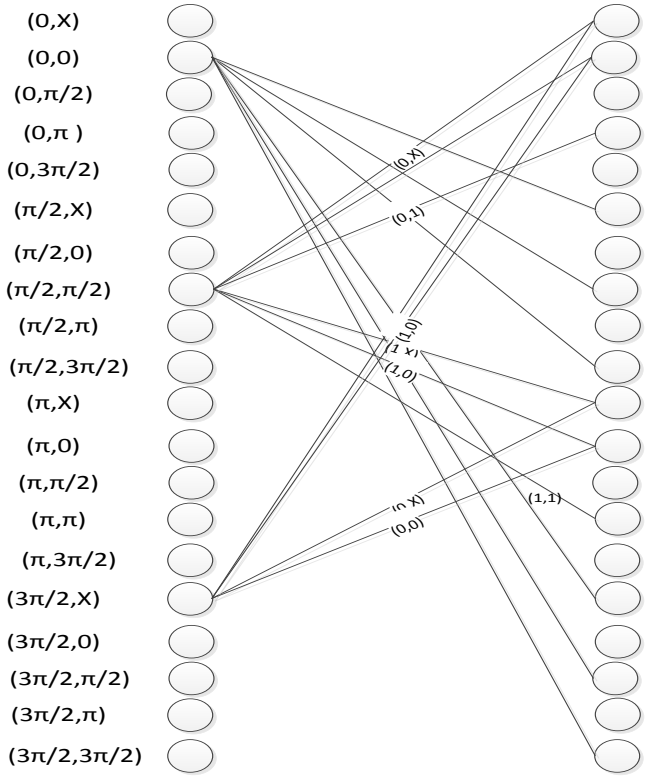

Figure 3-3. Trellis and transitions for a selected state.

proof-of-concept system in which two users occupy ten frequency bands. The system uses a fixed frame size of 1000 encoded bits, where encodeding is performed with a rate $1/2$ convolutional encoder with constraint length 7 of maximum free distance. The encoded bits are interleaved using a pseudo-random bit interleaver and the frame is transmitted over 10 dwell intervals. Each dwell interval contains $N = 5$ null symbols at the beginning and end of the sub-frame and $P = 5$ pilot symbols before and after the data frame. In effect, the number of symbol durations contained in each dwell interval is $L = 120$, where only $D = 100$ symbol durations contain data information.

We assume that each dwell interval experiences Rayleigh fading. We model A_1 and A_2 as circular-symmetric complex random variables that are constant over each

dwell interval but independent among dwell intervals. τ is uniformly distributed on $[0, T_s)$. When applying our scheme, we assume that all the parameters are unknown at the receiver and need to be estimated. However, for our comparison case, we assume that the parameters of the desired user is known a-priori at the receiver. For our scheme, we attempt to decode while we disregard the interference for the first 3 iterations. When decoding fails, then, we perform iterative interference mitigation and decoding.

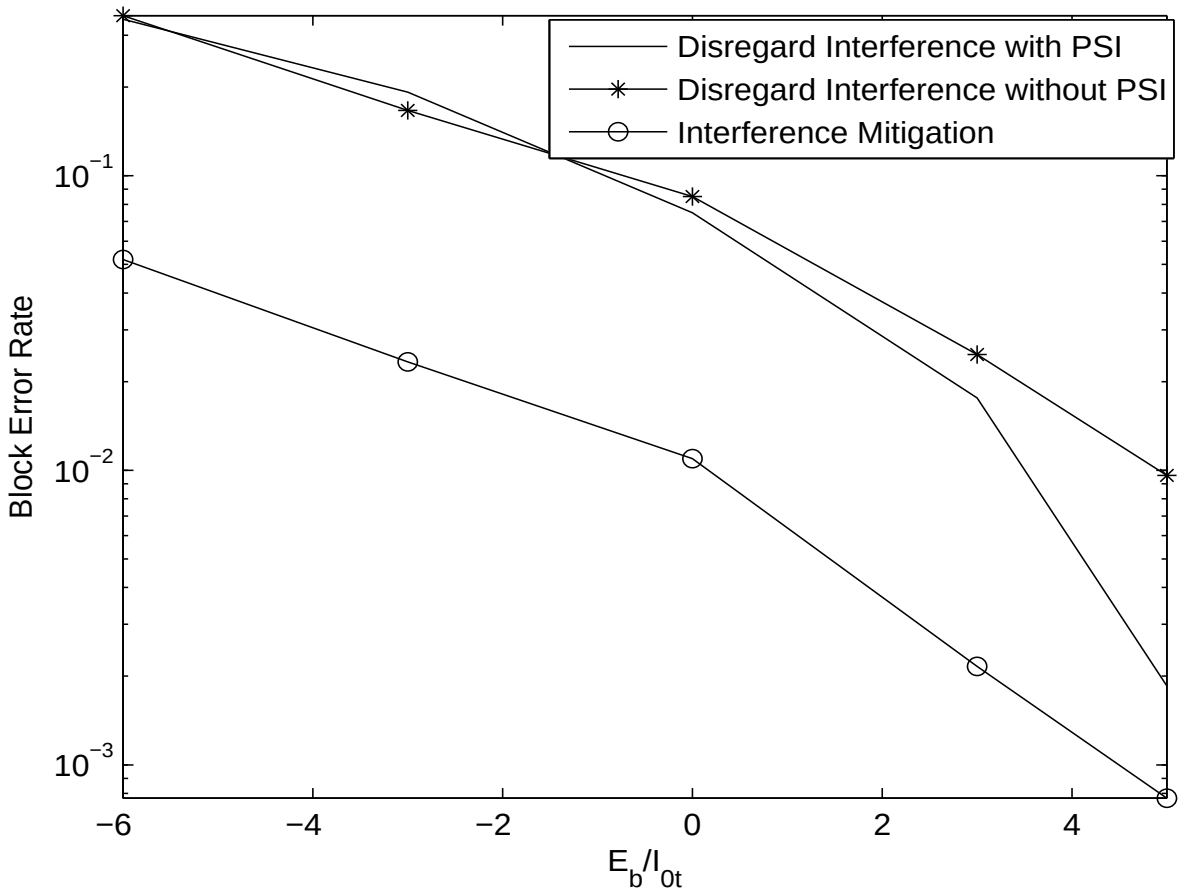

Figure 3-4. Comparison of schemes for $E_b/N_0 = 24$ dB across a range of Partial-Band Interference values.

Fig. 3-4 shows the performance of our scheme compared to using only the traditional scheme in the region of strong MAI. We see that our scheme significantly

outperforms the comparison case for all E_b/I_{0t}(Signal to Interference ratio)[2] . This is due to the fact that the estimate of the interference parameter is very good at high E_b/N_0 and allows accurate soft demodulation. The interference mitigation approach achieves an approximate order of magnitude improvement in the block error rate when compared to the system that ignores interference and has to estimate the desired user's channel. For a target rate of 10^{-2}, we get about a 3.5 dB improvement in the system's tolerance to interference compared to the case of perfect side information and 5 dB for the case where the receiver has to estimate the channel gain of the desired user.

Fig. 3-5 compares our approach for a fixed $E_b/I_{0t} = 5$ dB over a range of E_b/N_0. We see about a 4 dB improvement when we use the estimated side information and a smaller improvement when we use perfect CSI for the same target error rate of 10^{-2}. The important thing to note from this graph is the reduction in the error floor that comes from using our approach.

Fig. 3-6 shows the performance for fixed $E_b/I_{0t} = 0$ dB. We see that the target error rate of 10^{-2} is unachievable with the scheme that does not perform interference mitigation, even if perfect channel estimates are available for the desired user, but can be achieved with our approach.

Next, we look at a more realistic case where we have several users contending over 100 frequency bands. From Fig. 3-7, we see an increase in the number of users that can be supported at any given error rate. For a target error rate of 10^{-2}, interference mitigation allows for the system to support 18 users compared with 4 for a system using the traditional approach.

[2] Here, I_{0t} is defined as the spectral density that would exist if the interference were uniformly spread over the dwell interval

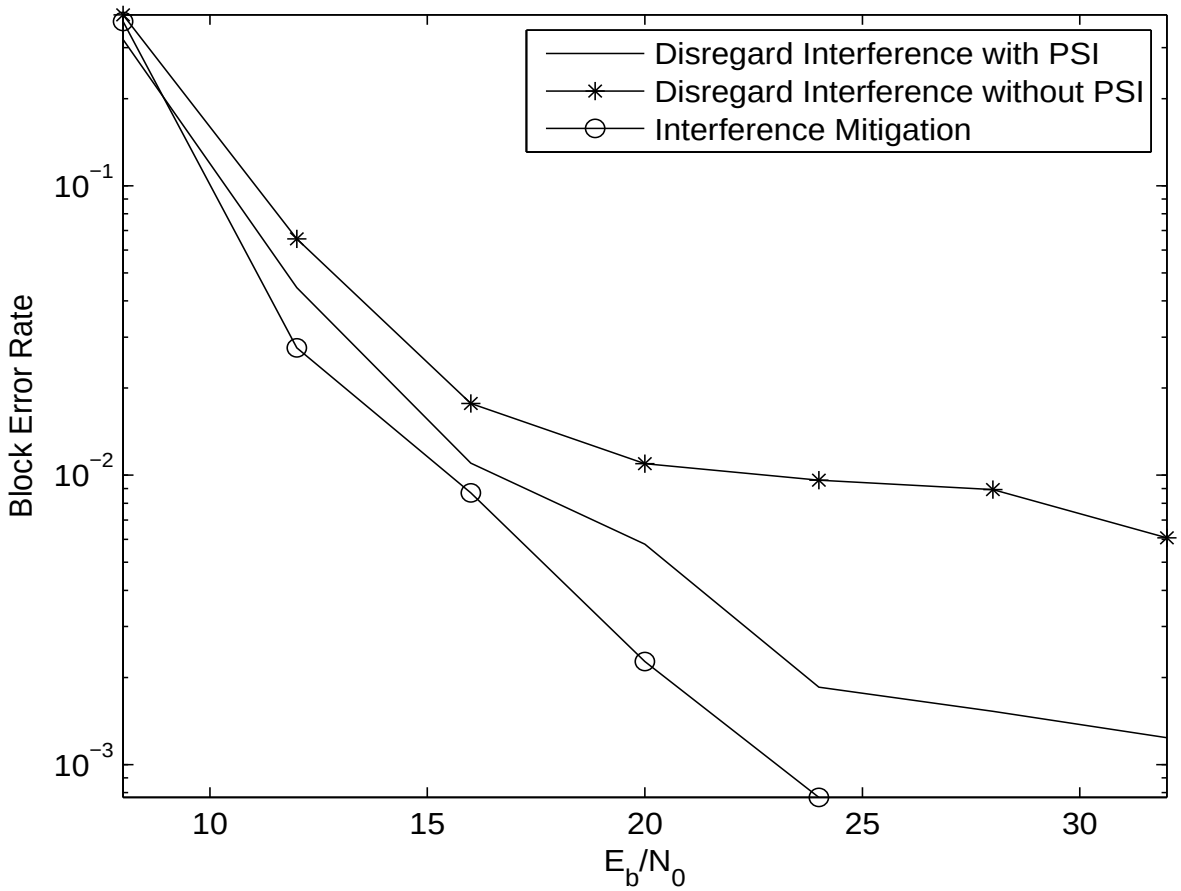

Figure 3-5. Comparison of schemes for $E_b/I_{0t} = 5$ dB across a range of E_b/N_0.

3.6 Summary

In this chapter, we developed an interference mitigation scheme for an FHSS system employing CPFSK. We exploit the structure of the interference in demodulation and utilize reliability estimates of the channel in the decoding process. The parameters of the interfering user are estimated in an iterative manner. The results show significant performance improvement over the traditional scheme. We observe an approximate order-of-magnitude improvement in block error rate for a $2-$user system when operating at $E_b/N_0 = 24$ dB for a variety of interference levels. When operating at an average E_b/I_{0t} of 5 dB, we observed a performance gain of approximately 4 dB in E_b/N_0 over the traditional scheme at a block error rate of 10^{-2}. For a system operating at $E_b/I_{0t} = 0$ dB,

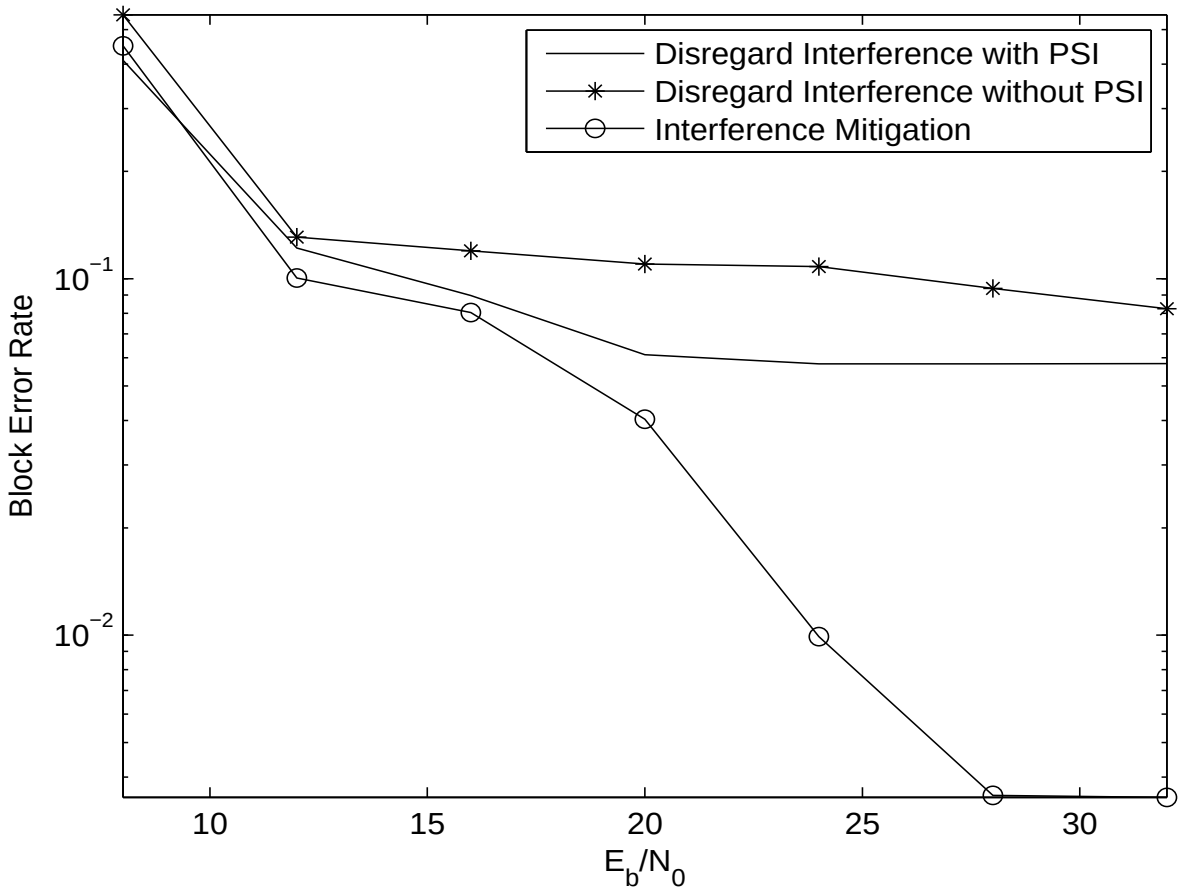

Figure 3-6. Comparison of schemes for $E_b/I_{0t} = 0$ dB across a range of E_b/N_0.

this error rate is unachievable using the traditional scheme but can be achieved using our interference mitigation scheme. Also, we show that interference mitigation allows for an increase of about 350% in the number of users that can be supported at a target block error rate of 10^{-2} for a system that consists of multiple users contending over 100 frequency bands.

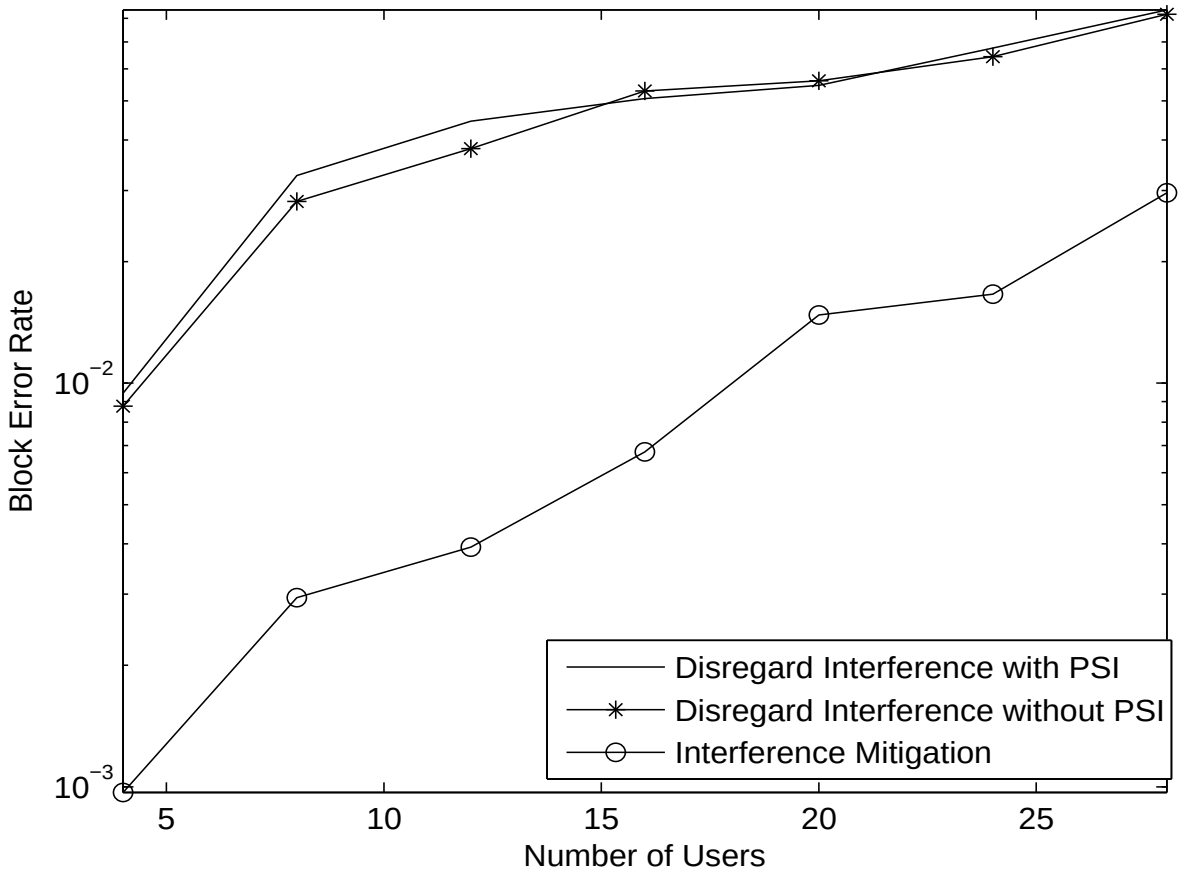

Figure 3-7. Comparison of schemes for $E_b/I_{0t} = 0$ dB and $E_b/N_0 = 24$ dB.

CHAPTER 4
ITERATIVE CHANNEL ESTIMATION AND PARTIALLY COHERENT DEMODULATION OF CPFSK IN TIME-SELECTIVE FADING CHANNELS

4.1 Introduction of Iterative Channel Estimation and Partially Coherent Demodulation of CPFSK in Time-Selective Fading Channels

System engineers face the challenge of how to design systems that operate in a very dynamic channel environment. Pilot symbol assisted modulation (PSAM) provides a way to continuously track the channel by using embedded known symbols for channel impulse response tracking [29, 34–36]. The pilot symbol insertion rate depends on the fade rate of the channel as postulated by Nyquist. Adaptive techniques like those proposed in [37–39] requires that information about the fade rate are constantly fed back from the receiver to the transmitter in order to continuously optimize the spacing between pilot symbols. When there is a mismatch between this insertion rate and the actual fade rate of the channel, the use of the channel gains derived from these pilot symbols in demodulation can adversely affect the system's performance.

In this chapter, we use iterative partially coherent demodulation and channel estimation to aid in decoding for a system employing CPFSK. We explore the use of sparser pilot symbol spacing and pilot insertion rates that are significantly lower than the rates specified by Nyquist. We show that for these scenarios the adaptive nature of the partially coherent scheme presented in this chapter allows for performance that is as good or better than either coherent or the noncoherent demodulation for most fading scenarios.

4.2 System Model

We consider a system that transmits using coded Continuous-Phase Frequency Shift Keying (CPFSK) over a time selective channel. The system model considered in this chapter is illustrated in Fig. 4-1. A sequence,$\{d_j\}$, of L data bits is encoded with a forward error-correction code. The encoded bits are then passed through an interleaver to generate a new sequence $\{b_j\}, 1 \leq j \leq L$. This new sequence is

then modulated into a sequence of CPFSK symbols and pilot symbol are inserted. During modulation and pilot symbol insertion, the input sequence is separated into M groups of contiguous bits. For each bit, $q_i, 1 \leq i \leq L/M$, in each of the contiguous bit-groups, a continuous time modulated signal $x_i(t)$ is chosen as the q_i^{th} signal from the set $\mathcal{S} = s_m(t), m = 0, ..., K-1$, where K is the alphabet size and

$$s_m(t) = \frac{1}{\sqrt{T_s}} \exp \frac{jh\pi(2m-1)t}{T_s}, \tag{4–1}$$

where h is the modulation index. In this chapter, for simplicity, we consider $K = 2$, that

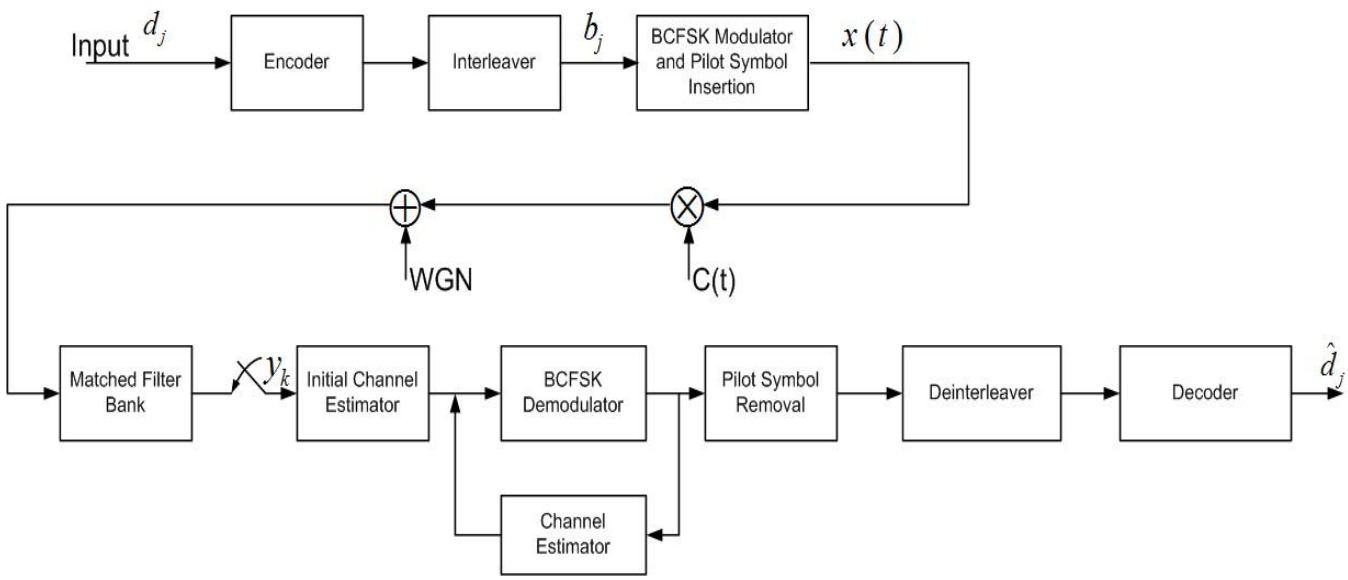

Figure 4-1. System model

is, the Binary-CPFSK case but this approach can also be extended to $K > 2$. In order to satisfy the continuous phase requirement for CPFSK, the phase of each symbol is accumulated as

$$\phi_{i+1} = \phi_i + (2q_i - (K-1))\pi h. \tag{4–2}$$

At the end of each bit-group, we insert data-dependent pilot symbols in order to force the phase to a predetermined phase state. Getting the accumulated phase to a known phase at the pilot symbol requires the addition of a number of symbols that

depends on h. For our case, 2 extra symbols are required, where the last symbol is the pilot symbol.

The pilot bits at the end of each bit-group provides the initial phase condition for the modulation of the next bit-group. This is done until the entire frame is modulated. At this point, we have $L + 2M$ symbols in the frame.

Let $c(t) = ae^{j\theta}$ be the complex value process that describes the behavior of the channel. Since we are considering a frequency non-selective flat fading channel, we model $c(t)$ as a zero mean low-pass Gaussian process. We assume that the real and imaginary parts of $c(t)$ are independent with autocorrelation

$$R_c(k) = \frac{1}{2} J_0(2\pi F_d T_s k), \tag{4–3}$$

where J_0 is the zeroth order Bessel function of the first kind, F_d is the relative Doppler between transmitter, and receiver and T_s is the symbol duration.

At the receiver,

$$y_k(t) = a_k e^{j\theta_k} \sqrt{E_s} e^{j\phi_k} x_k(t) + n_k(t), \qquad 1 \leq k \leq L + 2M,\ kT_s \leq t \leq (k+1)T_s. \tag{4–4}$$

This signal is passed through a bank of K matched filers to produce, in vector notation,

$$\boldsymbol{y} = ae^{j(\theta_k + \phi_k)} \sqrt{E_s} \boldsymbol{x} + \boldsymbol{n}. \tag{4–5}$$

where the elements of the vectors, $\boldsymbol{y}$, $\boldsymbol{x}$, and $\boldsymbol{n}$ can be represented as

$$y_m = ae^{j(\theta_k + \phi_k)} \sqrt{E_s} x_m + n_m \tag{4–6}$$

$$x_m = \int_0^{T_s} x(t) s_m(t) dt \tag{4–7}$$

$$n_m = \int_0^{T_s} n(t) s_m(t) dt \tag{4–8}$$

The noise vector $\boldsymbol{n}$ is Gaussian with covariance matrix, $\boldsymbol{R_n} = E(\boldsymbol{n}\boldsymbol{n}^H)$. The element of $\boldsymbol{R_n}$ are defined in terms of the sinc function as

$$r_{x,y} = N_0 \mathrm{sinc}(\pi(x-y)h)e^{j\pi(x-y)h}. \tag{4–9}$$

If we express the probability of the received vector, $\boldsymbol{y}$, that is the output of the K matched filters, in terms of $\boldsymbol{x}$, ϕ, θ and $a\sqrt{E}$, we get that

$$p(\boldsymbol{y}|\boldsymbol{x}, \phi.\theta, a\sqrt{E}) = \frac{1}{\pi^M \det(\boldsymbol{R_n})} \times \\ \exp -(\boldsymbol{y} - a\sqrt{E}\boldsymbol{x}e^{j(\phi+\theta)})^H \boldsymbol{R_n}^{-1}(\boldsymbol{y} - a\sqrt{E}\boldsymbol{x}e^{j(\phi+\theta)}). \tag{4–10}$$

Considering just the exponent, we have

$$-(\boldsymbol{y}^H \boldsymbol{R_n}^{-1}\boldsymbol{y} - a^2 E x^H \boldsymbol{R_n}^{-1} y + 2\,\mathrm{Re}(a\sqrt{E}e^{-j(\theta+\phi)}\boldsymbol{x}^H \boldsymbol{R_n}^{-1}\boldsymbol{y}). \tag{4–11}$$

where $\mathrm{Re}(\cdot)$ is the real component of the complex-valued argument.

Let us define the normalized covariance matrix, $\boldsymbol{P} = \boldsymbol{R_n}/(2\sigma^2)$. Then, we can see from (4–7), that when $x(t) = s_v(t)$, $\boldsymbol{x}$ is the vth column of $\boldsymbol{P}$. So, given $\boldsymbol{x} = p_v$, (4–11) becomes,

$$-\frac{(\boldsymbol{y}^H \boldsymbol{P}^{-1}\boldsymbol{y} + a^2 E \boldsymbol{x}^H \boldsymbol{P}^{-1} y)}{2\sigma^2} - \frac{\mathrm{Re}(ae^{-j(\theta+\phi)}\boldsymbol{x}^H \boldsymbol{P}^{-1}\boldsymbol{y})}{\sigma^2}. \tag{4–12}$$

For noncoherent demodulation, integrating (4–10) over the uniform random variable θ yields

$$p(\boldsymbol{y}|\boldsymbol{x}_v, \phi.\theta, a\sqrt{E}) = \frac{1}{(\pi 2\sigma^2)^M \det(\boldsymbol{P})} \\ \times \exp -\frac{(\boldsymbol{y}^H \boldsymbol{P}^{-1}\boldsymbol{y} + a^2 E \boldsymbol{x}^H \boldsymbol{P}^{-1}\boldsymbol{y})}{2\sigma^2} I_0\left(\frac{a\sqrt{E}}{\sigma^2}\,|y_v|\right), \tag{4–13}$$

where $I_0(\cdot)$ is the zeroth order Bessel function of the first kind and y_v is the vth column of $\boldsymbol{y}$.

If the channel phase is known, we can perform coherent demodulation, in which case we get

$$p(\boldsymbol{y}|\boldsymbol{x}_v, \phi.\theta, a\sqrt{E}) = \frac{1}{(\pi 2\sigma^2)^M \det(\boldsymbol{P})} \times \exp - \frac{(\boldsymbol{y}^H \boldsymbol{P}^{-1}\boldsymbol{y} + a^2 E \boldsymbol{x}^H \boldsymbol{P}^{-1}\boldsymbol{y})}{2\sigma^2} \times \exp\left(\frac{a\sqrt{E}}{\sigma^2}|y_v| \, cos(\angle y_v - \theta - \phi)\right), \quad (4\text{–}14)$$

where $\angle y_v$ refers to the angle at the output of the matched filter corresponding to x_v.

Assuming we have an imperfect phase estimate and a coherence parameter, α, that gives us information about the quality of the channel phase estimate, θ, then, given the estimates of the other parameters, $\boldsymbol{\lambda} = \{\boldsymbol{x}, \phi, \hat{\theta}, a\sqrt{E}\}$, evaluating (4–10) over the tikhonov density given in (2–26) yields

$$p(\boldsymbol{y}|\boldsymbol{x}_v, \phi.\theta, a\sqrt{E}) = \frac{1}{(2\pi)^{M+1}\sigma^{2M} \det(\boldsymbol{P}) I_0(\alpha)} \times \exp - \frac{(\boldsymbol{y}^H \boldsymbol{P}^{-1}\boldsymbol{y} + a^2 E \boldsymbol{x}^H \boldsymbol{P}^{-1}\boldsymbol{y})}{2\sigma^2} \times I_0\left(\frac{a\sqrt{E}}{\sigma^2}\sqrt{(\Upsilon_R)^2 + (\Upsilon_I)^2}\right), \quad (4\text{–}15)$$

where

$$\Upsilon_R = |y_v| \cos(\angle y_v - \phi) + \frac{\sigma^2 \alpha}{a\sqrt{E}} \cos\hat{\theta}$$

and

$$\Upsilon_I = |y_v| \sin(\angle y_v - \phi) + \frac{\sigma^2 \alpha}{a\sqrt{E}} \sin\hat{\theta}.$$

4.3 Channel Estimation

4.3.1 Initial Channel Estimation

At this stage, the only information available for channel estimation are those provided by the pilot symbols. With the knowledge of ϕ_k and $\boldsymbol{x}$ at these pilot positions,

we can generate local estimates of the channel at these positions. That is

$$\hat{c_p} = \boldsymbol{w}_p^T \boldsymbol{y}_p e^{-j\phi_p}, p = \{1, Y+1, 2Y+1, ..., (M-1)Y+1\}. \tag{4–16}$$

where p is pilot symbol position, Y is the pilot symbol spacing and $(\cdot)^T$ denotes the transpose operation. The vector $\boldsymbol{w}_p$ is defined as

$$w_{pi} = \begin{cases} 1 & \text{if } x_{pi} = 1, \\ 0 & \text{if otherwise,} \end{cases} \tag{4–17}$$

where x_{pi} and w_{pi} are the ith element of vectors $\boldsymbol{x}_p$ and $\boldsymbol{w}_p$ respectively.

Next, we generate estimates of the channel at all the other symbol position using the estimates at the pilot positions. In particular, we calculate the Minimum Mean Squared Error (MMSE) estimate of b_k given the channel realizations at the pilot positions. We can express every b_k as a linear combination of the c_p's. Mathematically,

$$\hat{b_k} = \sum_{p=1}^{M-1} h_p \hat{c_p}. \tag{4–18}$$

The solution to (4–18) decomposes to

$$\boldsymbol{h} = \boldsymbol{R}^{-1} \boldsymbol{r}. \tag{4–19}$$

where

$$\boldsymbol{h} = [h_0, h_1, h_2, ..., h_{M-1}]^T,$$

$$\boldsymbol{r} = [R_c(k-1), R_c(k-Y-1), ..., R_c(k-(M-1)Y-1)]^T,$$

and

$$\boldsymbol{R} =$$

$$\begin{pmatrix} R_c(0) & R_c(Y) & ... & R_c((M-1)Y) \\ R_c(Y) & R_c(0) & ... & R_c((M-2)Y) \\ R_c(2Y) & R_c(Y) & ... & R_c((M-3)Y) \\ ... & ... & ... & ... \\ R_c((M-1)Y)) & R_c((M-2)Y) & ... & R_c(0)) \end{pmatrix}$$

Once the channel autocorrelation, R_c, is known, the matrix inversion shown in (4–19) only needs to be performed once per packet. The linear gains are generated and applied to (4–18).

The evaluation of $\hat{c_k}$ and the calculation of its variance $\hat{\sigma_k}$ will be addressed in the next subsection.

4.3.2 Iterative Channel Estimation

After the first round of demodulation, channel estimation can be refined by feeding back hard symbol decisions $\boldsymbol{x}$ and symbol phase decisions ϕ_k. Armed with this knowledge, we can revisit (4–16) to generate local estimates of the channel at each symbol position. Specifically, we can write that

$$\hat{b_k} = \boldsymbol{w}_k^T \boldsymbol{y}_k e^{-j\phi_k}, \qquad 1 \leq k \leq L + 2M. \tag{4–20}$$

where $\boldsymbol{w}_k$ is similarly defined as in (4–16).

However, the estimates produced in (4–20) are noisy estimates. To reduce the amount of noise in these estimates, we pass it through a filter. The best linear MMSE estimate of the channel is given by

$$\hat{c_k} = \sum_{i=-\lfloor Q/2 \rfloor}^{\lfloor Q/2 \rfloor} \omega_i b_{k-i}, \qquad 1 \leq k \leq L + 2M. \tag{4–21}$$

Here, Q is the filter size and the ω_i's are defined as the coefficients of the filter derived by solving the Wiener-Hopf equations given by

$$\sum_{i=-\lfloor Q/2 \rfloor}^{\lfloor Q/2 \rfloor} \omega_i R_c[k-i] + 2\sigma^2 \omega_k = R_c[k]. \tag{4–22}$$

The weighted variance is calculated by

$$\hat{\zeta_k} = 0.5\frac{V_1}{V_1^2 - V_2}\sum_{i=-\lfloor Q/2 \rfloor}^{\lfloor Q/2 \rfloor} |\omega_i|(b_{k-i} - \hat{c_k}). \tag{4–23}$$

Here, $V_1 = \sum_{i=-\lfloor Q/2 \rfloor}^{\lfloor Q/2 \rfloor} |\omega_i|$ and $V_2 = \sum_{i=-\lfloor Q/2 \rfloor}^{\lfloor Q/2 \rfloor} \omega_i^2$. A table look-up is performed on this value to generate corresponding α's for all symbol positions.

Coherent decoding only occurs when the variance is equal to 0. This means that the channel is neither affected by fading nor channel noise. Since this situation never really occurs in practice, at each iteration, we decide whether to perform coherent or partially coherent demodulation depending on the overall quality of the channel as suggested by the average of all the $\hat{\zeta_k}$. If this average is greater than some empirically-determined threshold, we use partially coherent demodulation, else, we use coherent demodulation. In our simulations, we found out that a normalized variance threshold of 0.15 provides the best result across all fade rates.

4.4 Simulation Results

The performance of the partially coherent technique was examined by simulation and compared to the traditional coherent and noncoherent techniques. We evaluated the system for a fixed data length of 1000 encoded bits, where encoding is performed with a rate $1/2$ convolutional encoder of constraint length 7 of maximum free distance. $M = 10$ pilot symbols are placed in the frame for channel tracking to produce a pilot spacing of $Y = 100$.

Slow fading is assumed and we evaluate the channel performance for normalized fade rates $F_dT_s = 0.005$, $F_dT_s = 0.01$, $F_dT_s = 0.02$, and $F_dT_s = 0.04$. According to Nyquist, the pilot insertion rates for these fade rates should be $Y < 100$, $Y < 50$, $Y < 25$, and $Y < 12.5$ respectively. For all fade rates, the size of the Wiener filter used in channel estimation is $Q = 31$.

Seven demodulation and channel estimation iterations were performed and the Viterbi Algorithm was used to demodulate the frame on a trellis with the decoding

metrics given by (4–14) and (4–15) for the coherent and partially coherent schemes respectively.

The interesting thing to note from all the figures presented in this section is the adaptive nature of the partially coherent scheme. In Figs. 4-2 and 4-3, we see that the performance of the partially coherent scheme largely keeps in step with those of the coherent scheme. However, it outperforms the coherent scheme in the case of $F_d T_s = 0.01$ for large $E_b/N_0 (> 16dB)$. This is because at these fading rates, pilot symbols largely track the variations within the channel, and the partially coherent scheme assigns high confidence to the channel phase estimates generated in the system.

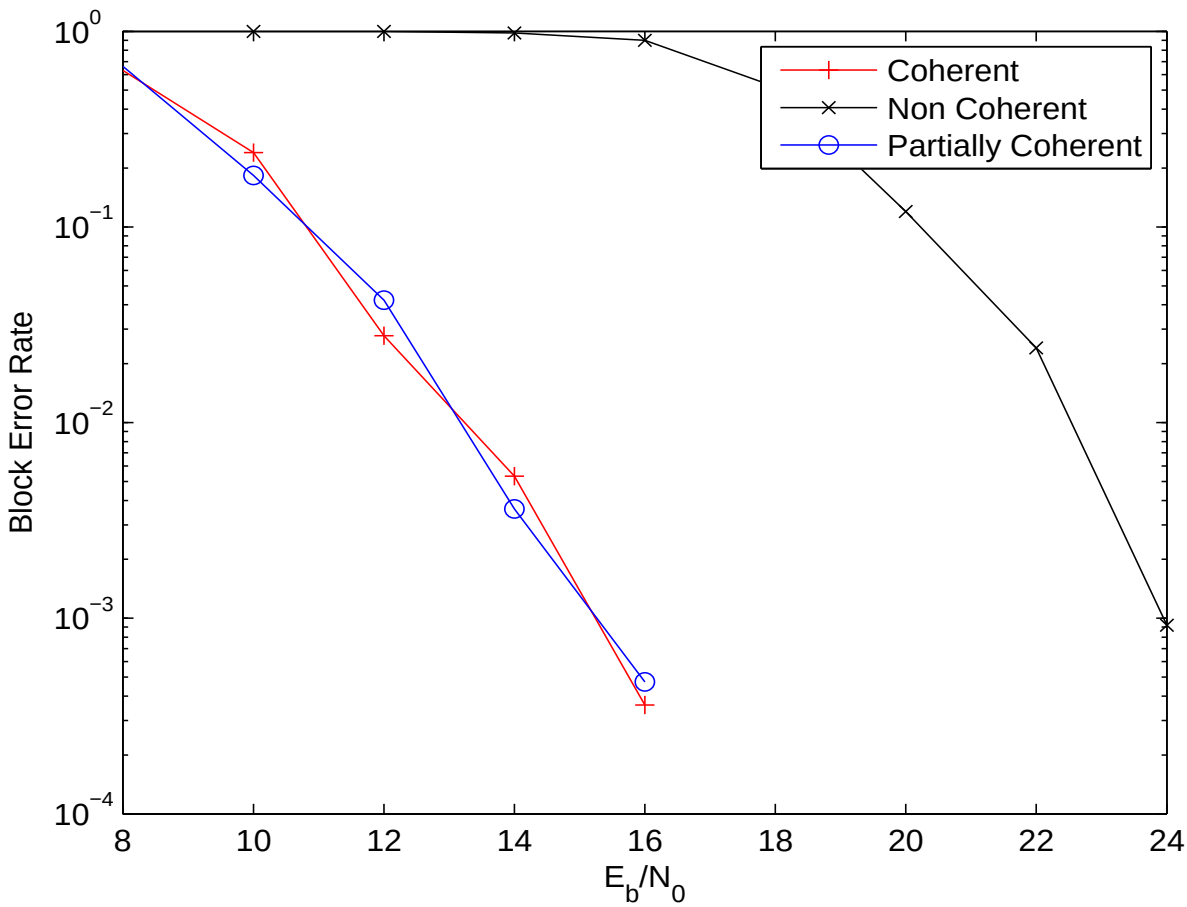

Figure 4-2. Comparison of demodulation schemes for $F_s T_s = 0.005$.

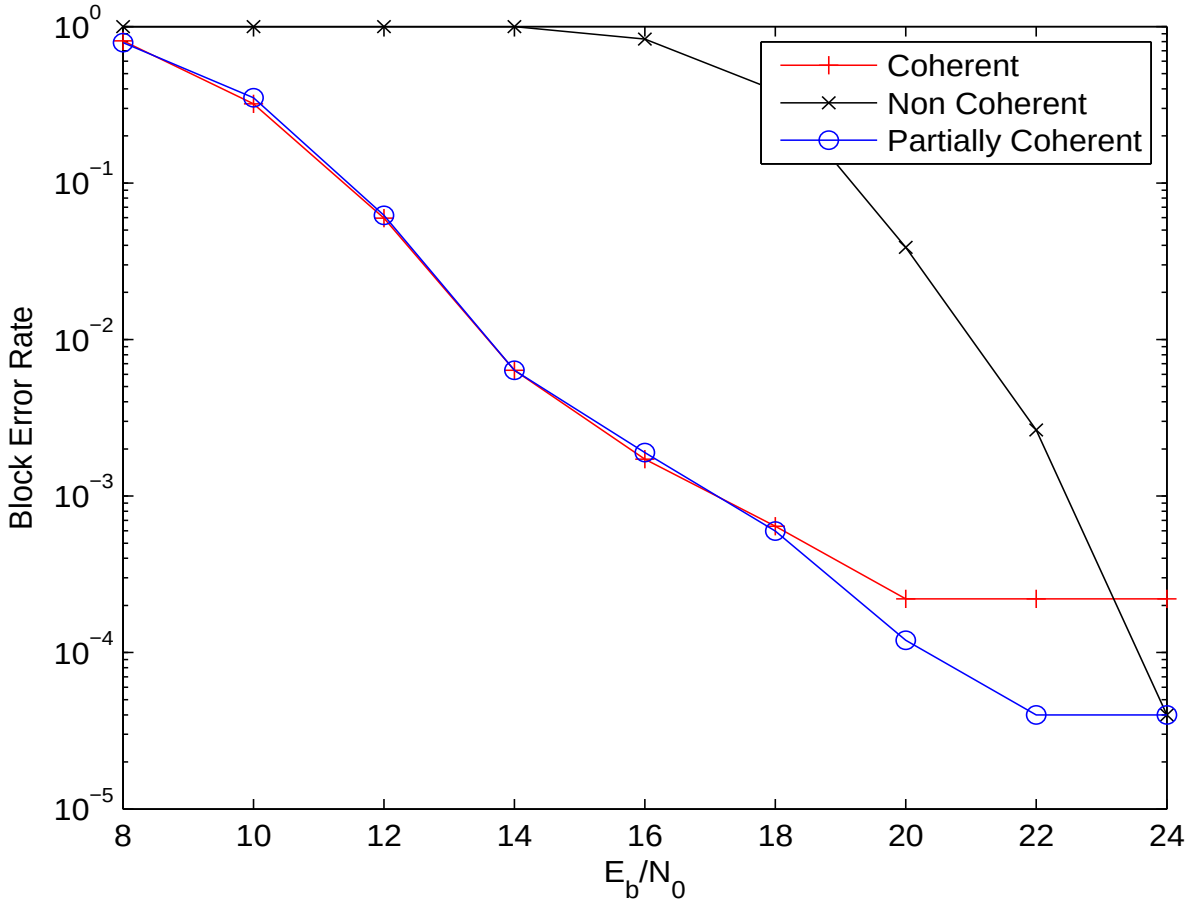

Figure 4-3. Comparison of demodulation schemes for $F_sT_s = 0.01$.

Fig. 4-4 and Fig. 4-5 tell a different story. We observe that for these fade rates, the performance of a system applying the coherent scheme is severely degraded. This is because the pilot symbols no longer provide reliable estimation about the variations in the channel. We observe that for $F_dT_s = 0.02$ and block error rate of 10^{-3}. partially coherent demodulation outperforms noncoherent demodulation by about 3 dB. This target error rate cannot be achieved in a system utilizing coherent demodulation. The partially coherent scheme also offers a slight advantage over the noncoherent scheme across all E_b/N_0 for $F_dT_s = 0.04$. We notice that at a block error rate of 10^{-2}, the partially

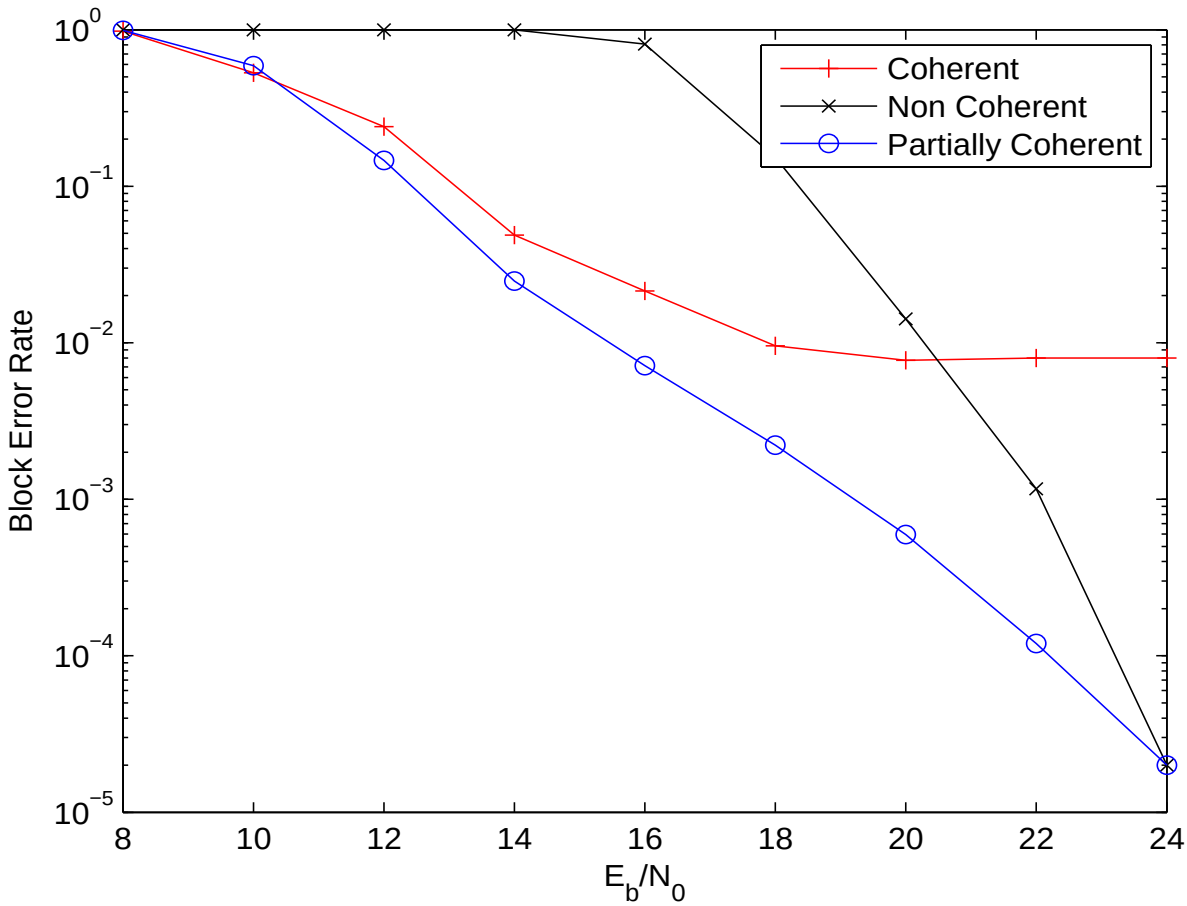

Figure 4-4. Comparison of demodulation schemes for $F_sT_s = 0.02$.

coherent scheme has about a 2 dB advantage over the noncoherent scheme. This error rate is unachievable using coherent demodulation.

Fig. 4-6 shows the block error rate as a function of E_b/N_0 for varying number of receiver iterations in a channel with a fixed fade rate of $FdTs = 0.005$. We observe that iterative demodulation provides an improvement in performance because it allows for more accurate channel estimates.

4.5 Summary

In this chapter, we have shown the performance improvement that is achievable through the use of partially coherent demodulation in a system employing binary

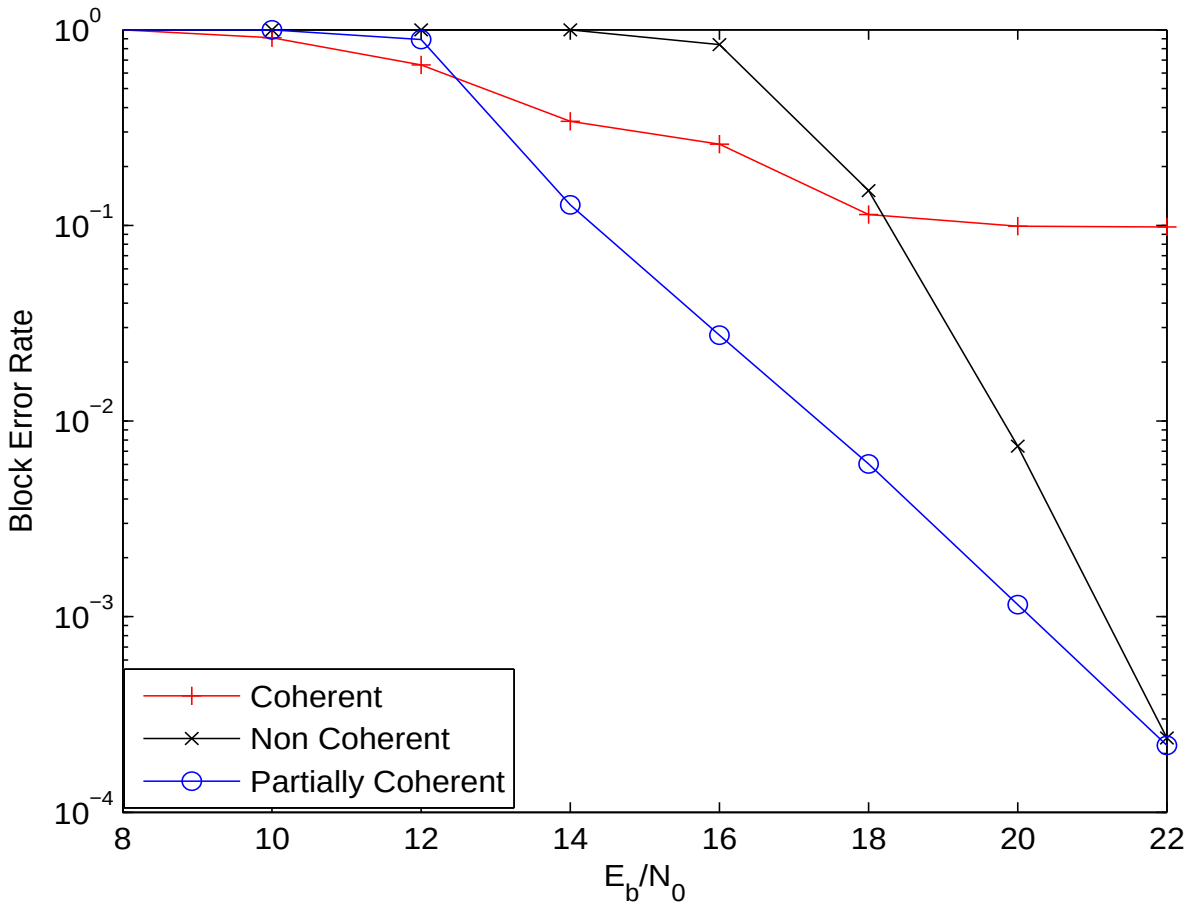

Figure 4-5. Comparison of demodulation schemes for $F_sT_s = 0.04$.

CPFSK. We have also shown that we can achieve performance gains of over 3 dB compared with the best of either noncoherent or coherent demodulation for pilot symbol insertion rates that are sparse compared to Nyquist.

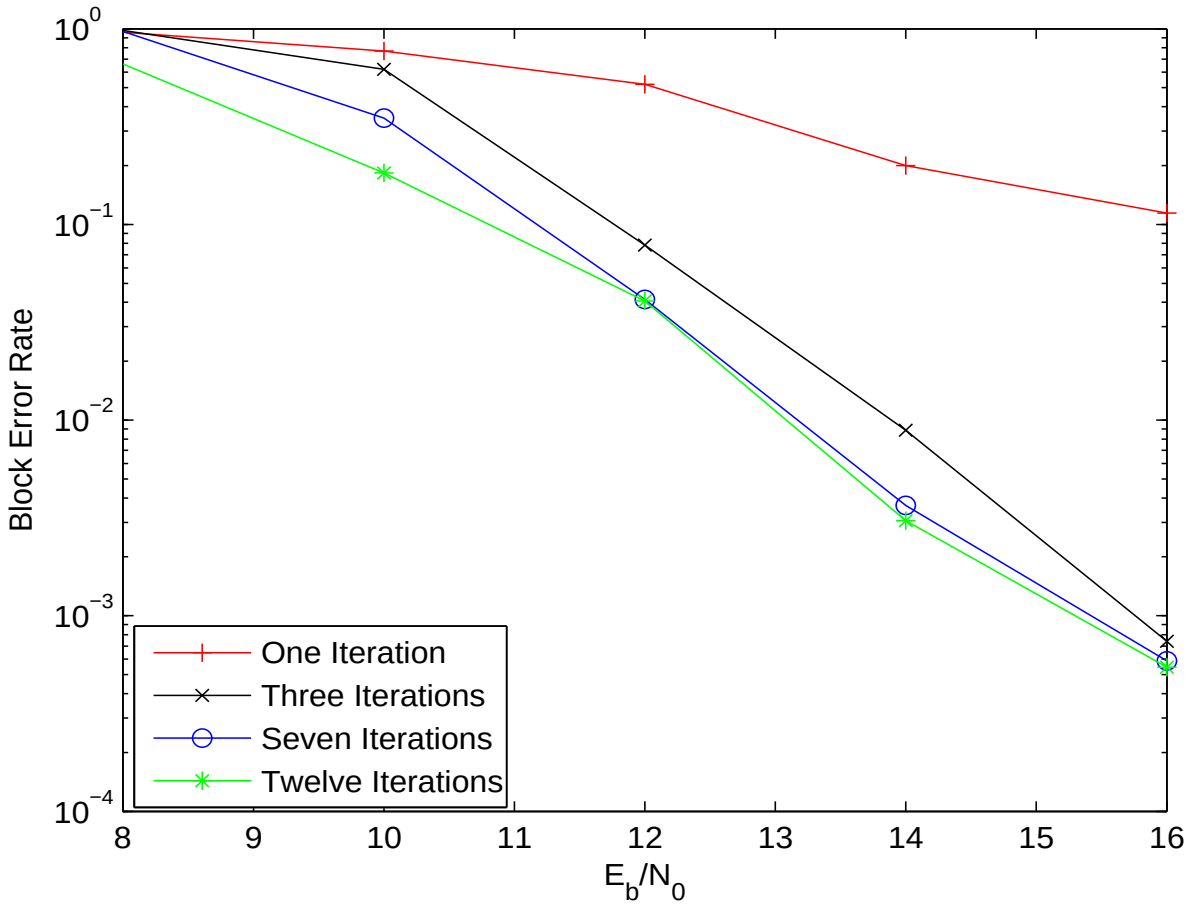

Figure 4-6. Block error rate vs. E_b/N_0 for varying number of iterations and $F_sT_s = 0.005$.

CHAPTER 5
LINK-LAYER THROUGHPUT OF FREQUENCY-HOPPING SYSTEMS WITH INTERFERENCE MITIGATION

5.1 Introduction of Link-Layer Throughput of Frequency-Hopping Systems with Interference Mitigation

In this section, we consider the improvement that is achieved in the data link layer as a result of interference mitigation on the physical layer. We present a simple system model and we use this to study what influence this physical-layer improvement has on the link-layer throughput.

We consider how interference information calculated in the interference mitigation algorithm of each node can be used to estimate of the average number of users in the system during a particular time period. This knowledge is used to develop a cross-layer protocol that dynamically varies the transmission probability in order to maximize aggregate system throughput.

5.2 System Model

We consider a system in which radios are distributed randomly in space. Consider a group of radios that are uniformly distributed within a circle of radius R. We seek to evaluate the aggregate system throughput which is defined as the average number of packets received per reception slot. It is also assumed that all the nodes possess the same transmit power. For a transmitter at a distance d, the received power is given by

$$P_{RX} = \frac{P_{TX} C_0 a}{d^\alpha},$$

where $d \in \{0, R\}$, C_0 is the path loss gain at the reference distance d_0, α is the path loss exponent which is assumed to be 2 for this study, and a is the Rayleigh fading gain.

For nodes uniformly distributed within a circle of radius R, the probability density function (pdf) of any point, d, from the center is given by

$$f_D(d) = \frac{2d}{R^2}, \qquad d \in \{0, R\}.$$

If we define a new variable $y = \frac{1}{d^2}$, we get that

$$f_Y(y) = \frac{2}{y^2 R^2}, , \qquad d \in \{R^{-2}, \infty\}.$$

Also, since a is Rayleigh distributed with pdf

$$f_A(a) = \frac{a}{\sigma^2} \exp\left(-\frac{a^2}{2\sigma^2}\right),$$

we get that the random variable $z = ay$, is distributed according to

$$f_Z(z) = \frac{\sigma}{z^2 R^2}\sqrt{\frac{\pi}{2}}, \qquad z \in \{0, \infty\}.$$

$f_Z(z)$ is the distribution of the received power.

For varying number of users, k, we simulated the fading and path loss effects in the presence of additive Gaussian noise. We look at two cases: one for which we perform interference mitigation and one for which we do not. We generate corresponding block error rates for both cases in a system that consists of K users contending over $F = 100$ frequency bands with average $E_b/N_0 = 24dB$. Selected values are presented in Table 5-1.

Table 5-1. Selected number of users and corresponding block error rates .

$C_0 = 0.9$, $R = 3d_0$		
	Probability of Block Error B_{ek}	
Number of Users, k	With Interference Mitigation	Without Interference Mitigation
1	0.0060	0.0061
2	0.0069	0.0107
4	0.0100	0.0225
6	0.0109	0.0358
8	0.0123	0.0491
20	0.0345	0.1576
40	0.0966	0.3668
60	0.1916	0.5605
80	0.2986	0.7002
100	0.4187	0.8156

5.3 Throughput Analysis

Given the probability of block error, we can derive the average system throughput of a system consisting of N nodes. We assume that all the nodes operate in half-duplex mode. We also assume that each node has a packet available for transmission. In order words, we operate under saturation conditions, in which the transmission queue for each node is always assumed to be non-empty. We assume that each node in the system transmits in a slot with the same probability p. It follows that the system throughput, S, defined as the number of nodes multiplied by the probability that a packet generated by any node, i, within an N-node network is successfully received by its intended receiver, $j \in N$, is given by

$$S(N,p) = N \sum_{k=1}^{N} \binom{N}{k} p^{k+1}(1-p)^{N-k+1}(1-B_{ek})J(N,k), \tag{5–1}$$

where B_{ek} is the probability of block error given k users in the system and

$$J(N,k) = \sum_{m=1}^{k} \frac{1}{m}\binom{k}{m}\left(\frac{1}{N-k}\right)^{m}\left(1-\frac{1}{N-k}\right)^{k-m}\frac{1}{1-\left(1-\frac{1}{N-k}\right)^{k}}$$

is the probability that the receiver is available for reception. In particular, it is assumed that, due to the asynchronous nature of packet transmission, if $n \in N$ users transmit to the same receiver within a reception interval, the receiver only receives from at most one transmitter. We compare the throughput of the mitigation and no mitigation cases as a function of p for several values of N in Fig. 5-1, 5-2, 5-3, 5-4, and 5-5. We see that interference mitigation results in a marked improvement in the maximum achievable throughput across all values of N. Table 5-3 presents this improvement across the values of N considered in this study.

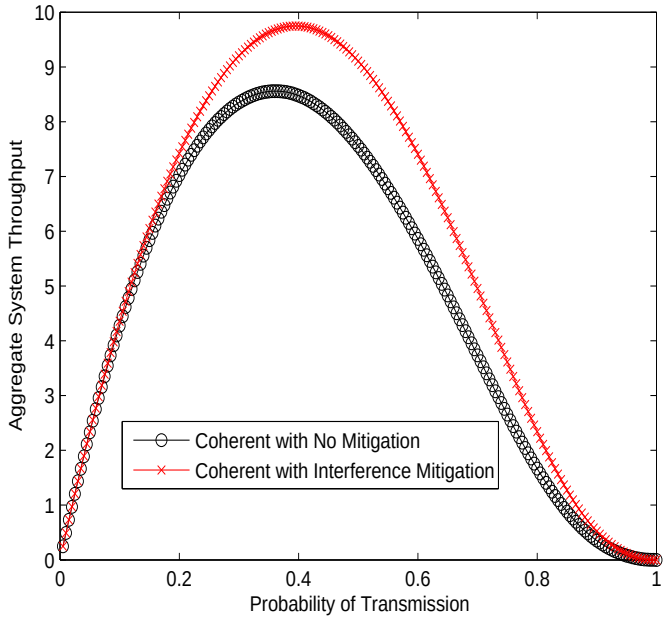

Figure 5-1. Throughput as a function of the transmission probability for a network consisting of 50 users.

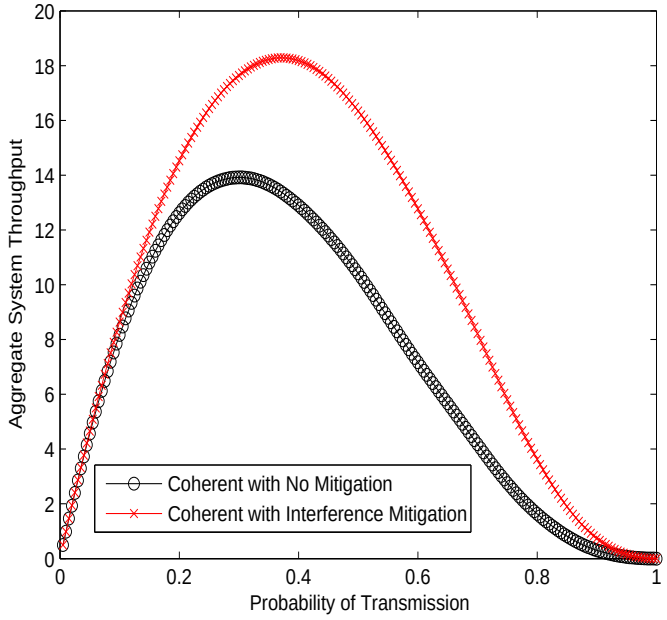

Figure 5-2. Throughput as a function of the transmission probability for a network consisting of 100 users.

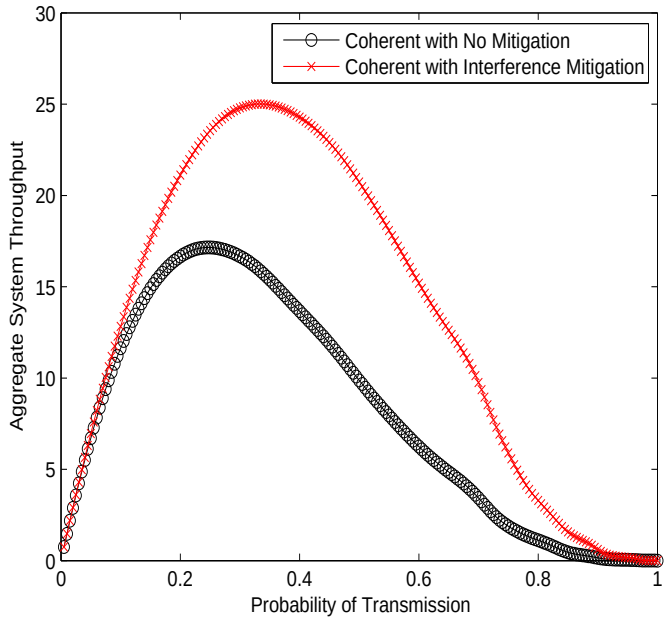

Figure 5-3. Throughput as a function of the transmission probability for a network consisting of 150 users.

Table 5-2. Comparison of the maximum achievable throughput for both cases.

	Maximum Achievable Throughput S_{max}		
N	With Interference Mitigation	Without Interference Mitigation	% Improvement
50	9.75	8.56	14%
100	18.29	13.92	31%
150	25.01	17.15	46%
200	30.21	19.21	57%
250	34.21	20.60	66%

We seek to choose the probability of transmission, p, of each node in order to maximize the system throughput. Maximizing Equation 5–1 with respect to p yields

$$\frac{dS(N,p)}{dp} = \sum_{k=1}^{N} \beta_{N,k} p^k (1-p)^{N-k+1} J(N,k) - \sum_{k=1}^{N} \alpha_{N,k} (1-p)^{N-k} p^{k+1} J(N,k) = 0, \quad (5\text{–}2)$$

where

$$\beta_{N,k} = (1+k)\binom{N}{k}(1-B_{ek}), \text{ and}$$

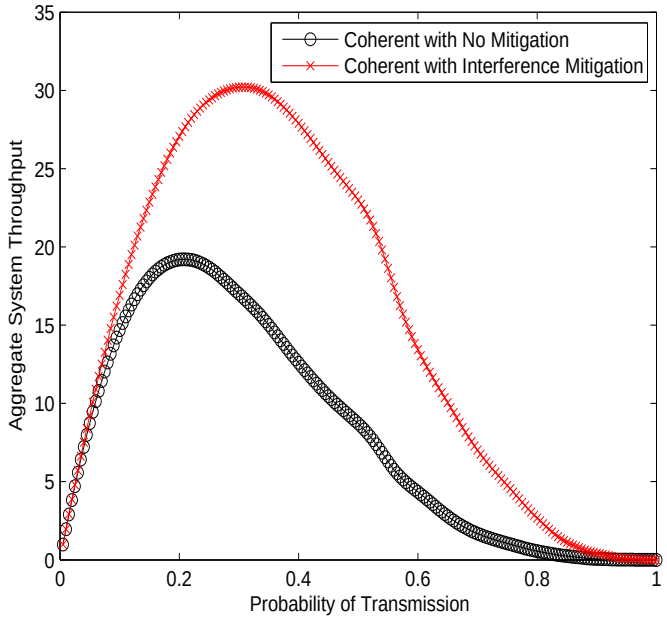

Figure 5-4. Throughput as a function of the transmission probability for a network consisting of 200 users.

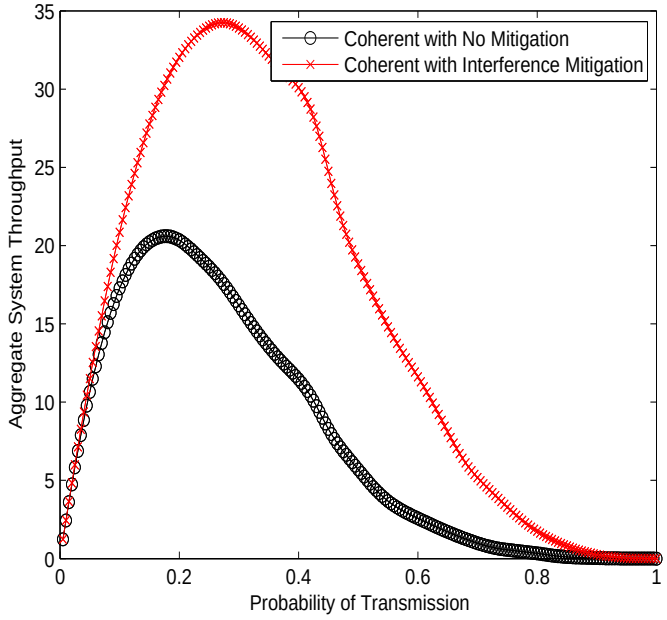

Figure 5-5. Throughput as a function of the transmission probability for a network consisting of 250 users.

$$\alpha_{N,k} = (N - k + 1)\binom{N}{k}(1 - B_{ek}).$$

This solution can be derived numerically.

Given an optimal p, for a given network scenario, we can employ a simple backoff window system where each node operating independently on its own clock, randomly waits for a random integer slot time $t \in (0, W - 1)$ before it transmits. According to [40], the backoff window size, W, is given by

$$W = \frac{2}{p} - 1, \tag{5–3}$$

rounded to the nearest integer. This guarantees that the system is operating at or close to its maximum achievable throughput. The optimal transmission probability p for the system being considered is presented in Fig. 5-6.

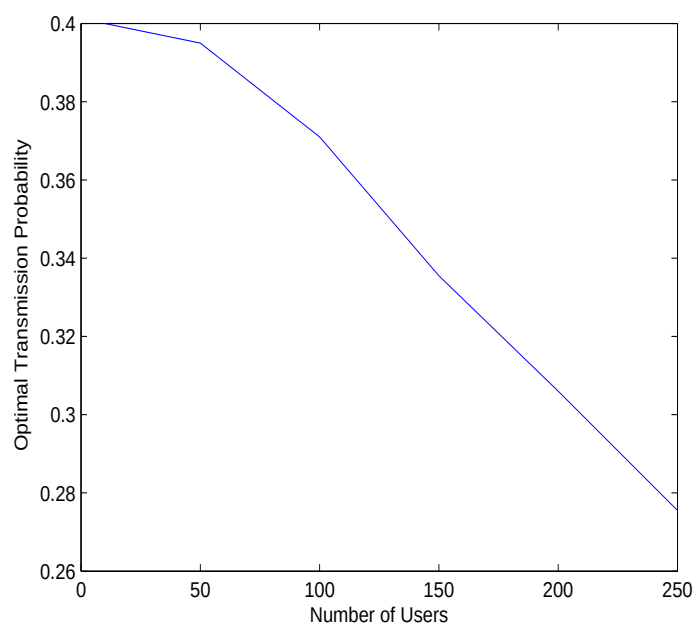

Figure 5-6. Optimal transmission probability as a function of the number of users in the system.

5.4 Cross-Layer Protocol

From (5–2), we see that the derivation of the optimal transmission probability is dependent on the number of users, N. This is information that is not readily available at each node since the network might change from time to time. However, we can use the observed interference activity at each node to derive an estimate of the number of users in the network. This allows us to use information derived in the interference mitigation algorithm to make decisions at the link layer.

Consider the physical layer setup considered in Chapter 2. Each node transmits a frame to the receiver over $D = 10$ dwell intervals. We also assume that the nodes contend over $F = 100$ frequency bands. Null bits are placed on the left and right side of the information transmitted over each dwell interval. Due to the asynchronous nature of transmission, we have $2D$ observations of the interference at the receiver. We decide that a dwell interval has been interfered with if the amplitude observed at the null positions on the left or/and right side exceeds a certain threshold.

Given N_a interferers, the probability that a dwell interval is detected to be hit from the left or right is given by

$$\text{Pr(detected hit)} = \bar{p} = \left(1 - \left(1 - \frac{1}{F}\right)^{N_a}\right)\Gamma$$

Here, $\Gamma = \text{Pr}(z > \tau)$. For this study, the threshold, $\tau = 0.1$.

Let us assume that after K observations, we have K_0, K_1, and K_2 dwell intervals with 0, 1, and 2 interferers respectively. It follows that the Maximum Log Likelihood estimate of N_a is given by

$$\frac{d}{dN_a}(\bar{p})^{2K_2}(2\bar{p} - 2\bar{p}^2)^{K_1}(\bar{p}^2 - 2\bar{p} + 1)^{K_0} = 0,$$

which yields

$$a^{N_a} = 1 - \frac{2K_2 + K_1}{2\Gamma(K_0 + K_1 + K_2)}.$$

Here, $a = \left(1 - \frac{1}{F}\right)$.

The estimate of the number of active nodes is given by

$$\tilde{N}_a = \left\lfloor \frac{\log\left(1 - \frac{2K_2+K_1}{2\Gamma(K_0+K_1+K_2)}\right)}{\log(a)} + 0.5 \right\rfloor. \tag{5–4}$$

5.5 Results and Discussion

In Figs. 5-7, 5-9, 5-11, 5-13, and 5-15, we present results that show how the throughput evolves as we dynamically vary the transmission probability based on this information for different system scenarios. Table 5-3 shows a summary of how well this cross-layer approach performs with regards to achieving the maximum system throughput in each scenario. The performance of the scheme that dynamically varies the transmission probability achieves a throughput that is within 6.6% of the optimal value for all values of N considered.

We also present results in Figs. 5-8, 5-10, 5-12, 5-14, and 5-16, that show the evolution of the average transmission probability across all the nodes over time. The horizontal line shows the optimal transmission probability in each scenario.

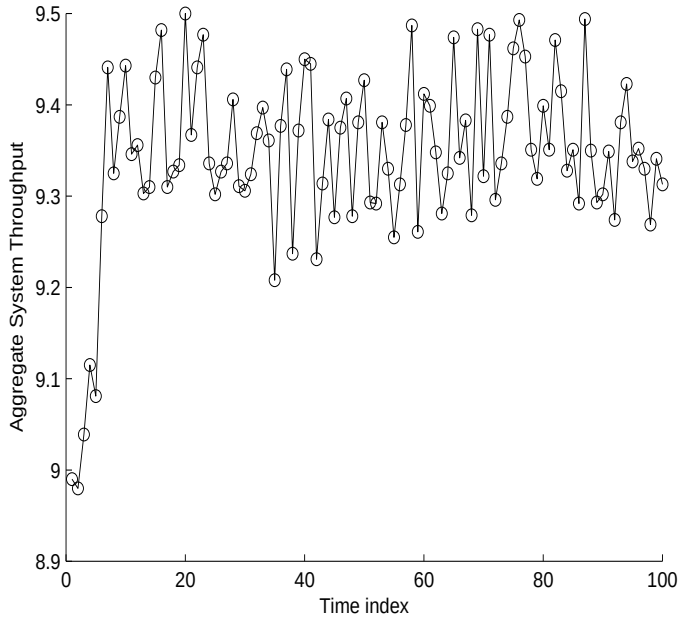

Figure 5-7. Throughput evolution over time, $N = 50$ users.

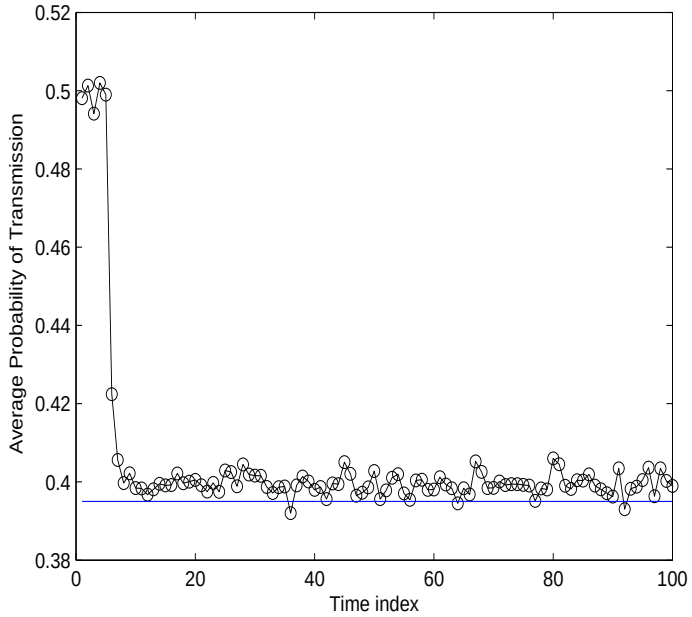

Figure 5-8. Evolution of average transmission probability over time, $N = 50$ users.

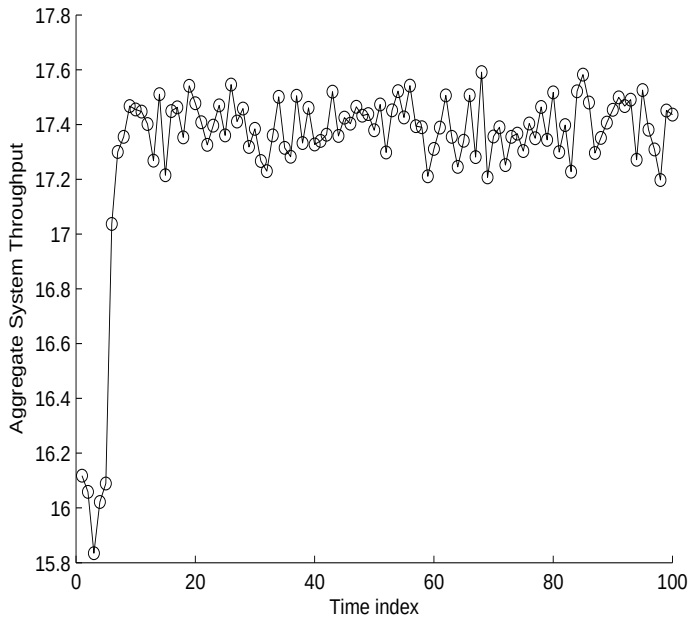

Figure 5-9. Throughput evolution over time, $N = 100$ users.

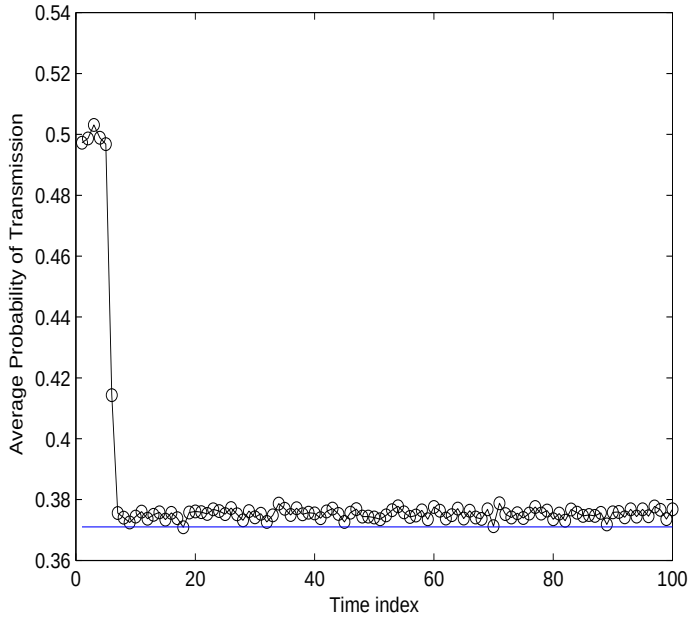

Figure 5-10. Evolution of average transmission probability over time, $N = 100$ users.

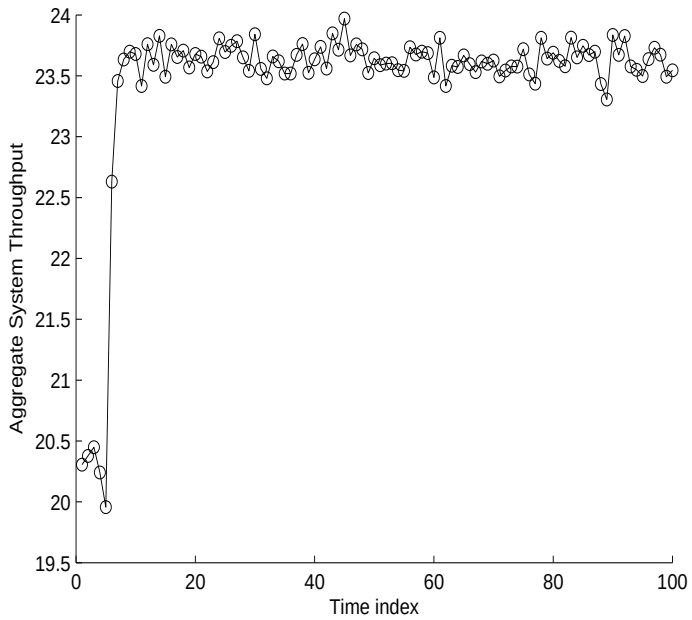

Figure 5-11. Throughput evolution over time, $N = 150$ users.

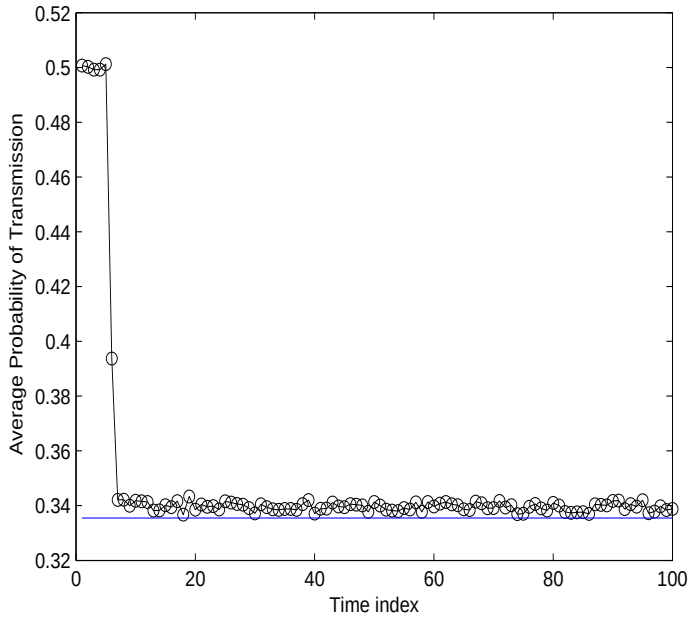

Figure 5-12. Evolution of average transmission probability over time, $N = 150$ users.

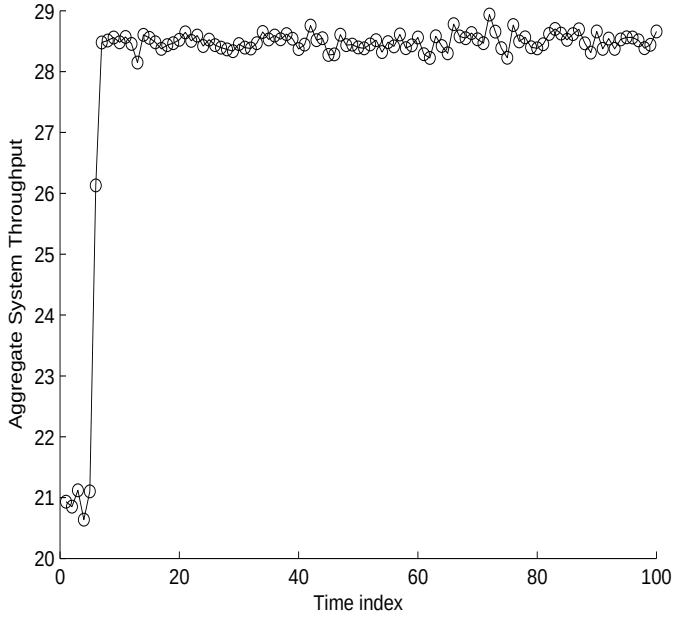

Figure 5-13. Throughput evolution over time, $N = 200$ users.

Table 5-3. Throughput comparison table.

N	Maximum Achievable Throughput S_{max}	Simulation Throughput	% Difference
50	9.75	9.34	4.2%
100	18.29	17.39	4.9%
150	25.01	23.58	5.7%
200	30.21	28.51	5.6%
250	34.25	31.98	6.6%

5.6 Summary

In this section, we performed a study that showed improvements in throughput as a result of interference mitigation in the physical layer. We also present a new technique that uses local information about interference at each receiver to estimate the number of users operating in the system at any particular time. We show that by using this information to modify its transmission probability, we can get performance that is close to the maximum achievable throughput.

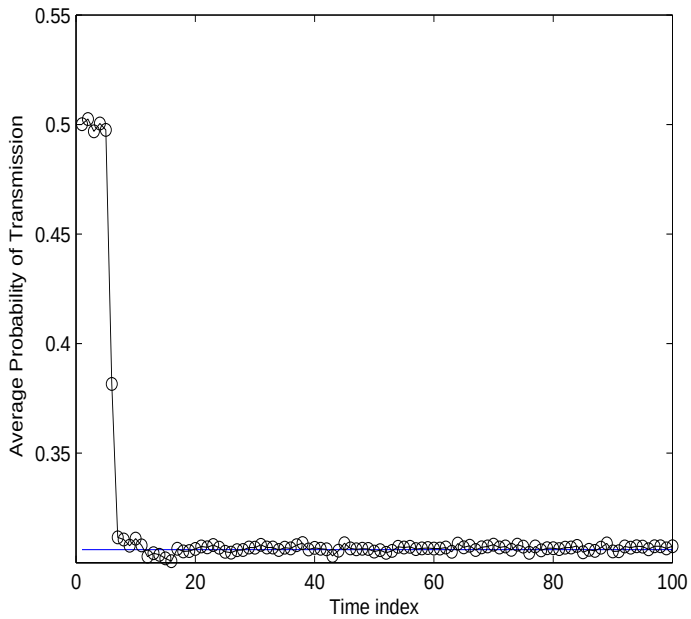

Figure 5-14. Evolution of average transmission probability over time, $N = 200$ users.

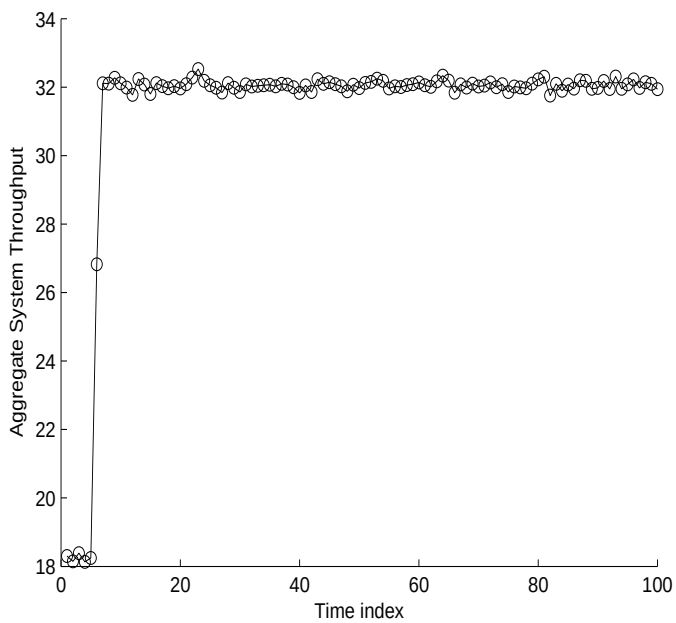

Figure 5-15. Throughput evolution over time, $N = 250$ users.

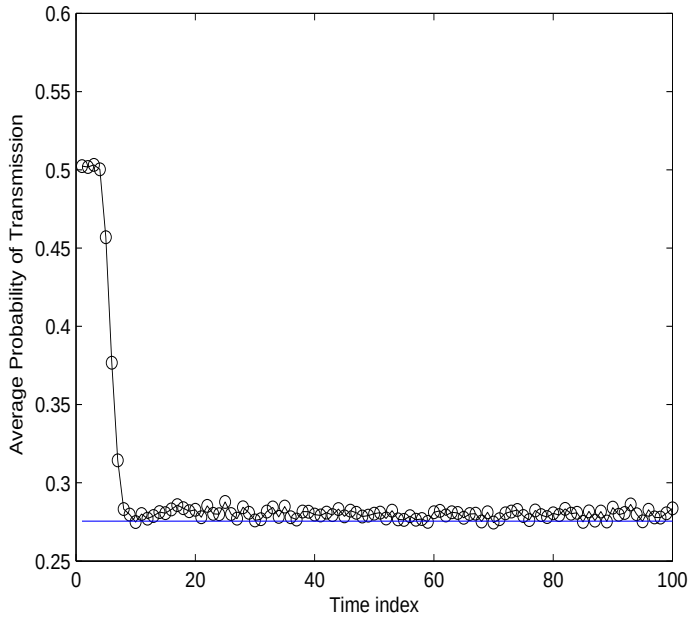

Figure 5-16. Evolution of average transmission probability over time, $N = 250$ users.

CHAPTER 6
CONCLUSIONS

In this Dissertation, we have developed techniques that use iterative partially coherent demodulation for systems operating in channels with multiple access interference and/or channel fading. In Chapter 2, we apply this approach to an interference mitigation scheme for use in a frequency-hopping spread-spectrum system that uses frequency shift key modulation. We show that applying partially coherent demodulation in an iterative manner can significantly improve the performance of a system in terms of block error rates and the multi-user capability of the system. We have also shown the calculation of a coherence parameter that serves as a measure of the reliability of the channel estimates.

Next, we considered interference mitigation in a system that employs frequency hopping with continuous-phase frequency shift keying. Interference mitigation for this type of system presents a unique challenge because the modulation is not memoryless. We presented a iterative channel estimation and demodulation scheme that provides performance gains in terms of the block error rates and multi-user access capability of the system.

We have also considered the use of iterative partially coherent demodulation in a frequency non-selective time varying channel. We show that this demodulation approach is adaptive to changing channel conditions. In particular, we showed performance improvements in block error rates when the pilot symbol insertion rate is lower than the Nyquist rate.

Finally, we evaluated the effect of these interference mitigation schemes on link-layer throughput for a simple slotted MAC protocol. The results show that interference mitigation significantly improves the aggregate system throughput for the frequency hopping systems. We have also presented a novel cross-layer approach in which the system throughput is approximately maximized by adapting each node's transmission

probability based on information it estimates in the the physical layer about the number of interferers it observes while it is in reception mode.

REFERENCES

[1] C. Frank and M. Pursley, "On the statistical dependence of hits in frequency-hop multiple access," *Communications, IEEE Transactions on*, vol. 38, no. 9, pp. 1483 –1494, sep 1990.

[2] T. G. Macdonald and M. B. Pursley, "Staggered interleaving and iterative errors-and-erasures decoding for frequency-hop packet radio," *IEEE Trans. Wireless Commun.*, vol. 1, pp. 92–98, Jan. 2003.

[3] U. Timor, "Improved decoding scheme for frequency-hopped multilevel FSK system," *Bell Syst. Tech. Journ.*, vol. 59, pp. 1839–1855, 1980.

[4] ——, "Multistage decoding of frequency-hopped FSK system," *Bell Syst. Tech. Journ.*, vol. 60, pp. 471–483, 1981.

[5] T. Mabuchi, R. Kohno, and H. Imai, "Multiuser detection scheme based on canceling cochannel interference for mfsk/fh-ssma system," *IEEE J. Sel. Areas Commun.*, vol. 12, no. 4, pp. 593–604, May 1994.

[6] U.-C. Fiebig, "Iterative interference cancellation for ffh/mfsk ma systems," *IEE Proc.–Commun.*, vol. 143, no. 6, pp. 380–388, Dec. 1996.

[7] K. Halford and M. Brandt-Pearce, "Multistage multiuser detection for FHMA," *IEEE Trans. Commun.*, vol. 48, no. 9, pp. 1550–1562, Sept. 2000.

[8] K. Hamaguchi, L.-L. Yang, and L. Hanzo, "Multi-stage multi-user detection assisted fast-fh/mfsk," *IEE Electronics Letters*, vol. 39, no. 4, pp. 399–400, Feb. 2003.

[9] N. Sharma, H. El Gamal, and E. Geraniotis, "Multiuser demodulation and iterative decoding for frequency-hopped networks," *IEEE Trans. Commun.*, vol. 49, no. 8, pp. 1437–1446, Aug. 2001.

[10] N. Sharma and E. Geraniotis, "Soft multiuser demodulation and iterative decoding for fh/ssma with a block turbo code," *IEEE Trans. Commun.*, vol. 51, no. 9, pp. 1561–1570, Sept. 2003.

[11] P.-P. Liang and W. Stark, "Iterative multiuser detection for turbo-coded FHMA communications," *IEEE J. Sel. Areas Commun.*, vol. 19, no. 9, pp. 1810–1819, Sept. 2001.

[12] J. Gass, J.H., P. Curry, and C. Langford, "An application of turbo trellis-coded modulation to tactical communications," in *Proc. 1999 IEEE Military Commun. Conf.*, vol. 1, 31 Oct.-3 Nov. 1999, pp. 530–533vol.1.

[13] C. W. Baum and M. B. Pursley, "Erasure insertion in frequency-hop communications with fading and partial-band interference," *IEEE Trans. Vehic. Technol.*, vol. 46, pp. 949–956, Nov. 1997.

[14] ——, “Bayesian generation of dependent erasures for frequency-hop communications and fading channels,” *IEEE Trans. Commun.*, vol. 44, pp. 1720–1729, Dec. 1996.

[15] ——, “Bayesian methods for erasure insertion in frequency-hop communication systems with partial-band interference,” *IEEE Trans. Commun.*, vol. 40, pp. 1231–1238, July 1992.

[16] A. Viterbi, “Phase-locked loop dynamics in the presence of noise by fokker-planck techniques,” *Proceedings of the IEEE*, vol. 51, no. 12, pp. 1737 – 1753, dec. 1963.

[17] S. Misra, A. Swami, and B. Chen, “Decision fusion in large sensor networks using partially coherent and noncoherent strategies,” in *Military Communications Conference, 2007. MILCOM 2007. IEEE*, oct. 2007, pp. 1 –7.

[18] T. Eng and L. Milstein, “Partially coherent ds-ss performance in frequency selective multipath fading,” *Communications, IEEE Transactions on*, vol. 45, no. 1, pp. 110 –118, jan 1997.

[19] M. Smadi, “Performance analysis of partially coherent frequency-selective channels with doppler shift,” in *Personal, Indoor and Mobile Radio Communications, 2006 IEEE 17th International Symposium on*, sept. 2006, pp. 1 –5.

[20] B. Zhang and K. Kiasaleh, “Partially-coherent receivers architectures for qam communications in the presence of non-constant phase estimation error,” *Wireless Communications, IEEE Transactions on*, vol. 8, no. 2, pp. 568 –573, feb. 2009.

[21] X. Tan and J. M. Shea, “Iterative detection and estimation for multiple access interference mitigation in asynchronous frequency-hop spread spectrum,” in *Proc. 2006 IEEE Military Commun. Conf.*, Washington, DC, Oct. 2006, pp. 1–7.

[22] ——, “An EM approach to multiple-access interference mitigation in asynchronous slow FHSS systems,” *IEEE Trans. Wireless Commun.*, vol. 7, no. 7, pp. 2661–2670, July 2008. [Online]. Available: http://wireless.ece.ufl.edu/jshea/pubs/xing_twireless07.pdf

[23] M. K. Simon, S. M. Hinedi, and W. C. Lindsey, *Digital Communication Techniques*. Prentice Hall, 1994.

[24] M. Simon and D. Divsalar, “Multiple symbol partially coherent detection of mpsk,” *Communications, IEEE Transactions on*, vol. 42, no. 234, pp. 430 –439, feb/mar/apr 1994.

[25] S. El-Khamy, S. Shaaban, and E. Thabet, “Partially coherent detection of continuous phase chirp (cpcm) signals,” in *Radio Science Conference, 1996. NRSC ’96., Thirteenth National*, mar 1996, pp. 485 –495.

[26] J. G. Proakis, *Digital Communications*, 4th ed. McGraw-Hill, 2000.

[27] D. Torrieri, S. Cheng, and M. Valenti, “Robust frequency hopping for interference and fading channels,” *Communications, IEEE Transactions on*, vol. 56, no. 8, pp. 1343 –1351, august 2008.

[28] ——, “Robust frequency-hopping system for channels with interference and frequency-selective fading,” in *Communications, 2007. ICC ’07. IEEE International Conference on*, june 2007, pp. 4481 –4487.

[29] M. C. Valenti and B. D. Woerner., “Iterative channel estimation and decoding of pilot symbol assisted turbo codes over flat-fading channels,” *IEEE J. Sel. Areas Commun.*, vol. 19, no. 9, pp. 1697–1705, September 2001.

[30] W. C. Lindsey, “Phase-shift-keyed signal detection with noisy reference signals,” *IEEE Trans. Aerosp. Electron. Syst.*, vol. AES-2, no. 4, pp. 393–401, July 1966.

[31] L. R. Bahl, J. Cocke, F. Jelinek, and J. Raviv, “Optimal decoding of linear codes for minimizing symbol error rates,” *IEEE Trans. Inform. Theory*, vol. 20, no. 2, pp. 284–287, Mar. 1974.

[32] D. Torrieri, S. Cheng, and M. Valenti, “Robust frequency-hopping system for channels with interference and frequency-selective fading,” in *Communications, 2007. ICC ’07. IEEE International Conference on*, june 2007, pp. 4481 –4487.

[33] O. Adeladan and J. Shea, “Interference mitigation with partially coherent demodulation in a slow frequency-hopping spread-spectrum system,” in *Military Communications Conference, 2009. MILCOM 2009. IEEE*, oct. 2009, pp. 1 –7.

[34] J. Cavers, “An analysis of pilot symbol assisted modulation for rayleigh fading channels [mobile radio],” *Vehicular Technology, IEEE Transactions on*, vol. 40, no. 4, pp. 686 –693, nov 1991.

[35] J.-H. Kim, P. Ho, and P. Goud, “Performance of binary cpm schemes in frequency selective fading channels with pilot symbol assisted detection,” *Communications, IEE Proceedings-*, vol. 144, no. 3, pp. 191 –198, jun 1997.

[36] Y.-S. Kim, C.-J. Kim, G.-Y. Jeong, Y.-J. Bang, H.-K. Park, and S. S. Choi, “New rayleigh fading channel estimator based on psam channel sounding technique,” in *Communications, 1997. ICC 97 Montreal, ’Towards the Knowledge Millennium’. 1997 IEEE International Conference on*, vol. 3, jun 1997, pp. 1518 –1520 vol.3.

[37] M. Karami, A. Olfat, and N. Beaulieu, “Pilot symbol assisted adaptive modulation for ofdm systems with imperfect channel state information,” in *Global Telecommunications Conference (GLOBECOM 2010), 2010 IEEE*, dec. 2010, pp. 1 –6.

[38] K. Yadav, N. Singh, and M. Srivastava, “Analysis of adaptive pilot symbol assisted modulation with optimized pilot symbol spacing for rayleigh fading channel,” in *Signal Processing, Communications and Networking, 2008. ICSCN ’08. International Conference on*, jan. 2008, pp. 405 –410.

[39] X. Cai and G. Giannakis, “Adaptive psam accounting for channel estimation and prediction errors,” *Wireless Communications, IEEE Transactions on*, vol. 4, no. 1, pp. 246 – 256, jan. 2005.

[40] G. Bianchi, L. Fratta, and M. Oliveri, “Performance evaluation and enhancement of the csma/ca mac protocol for 802.11 wireless lans,” in *Personal, Indoor and Mobile Radio Communications, 1996. PIMRC’96., Seventh IEEE International Symposium on*, vol. 2, oct 1996, pp. 392 –396 vol.2.

[41] J. Gass, J.H. and M. Pursley, “A comparison of frequency-hop and direct-sequence spread-spectrum communications,” in *Tactical Communications Conference, 1996., Proceedings of the 1996*, apr-2 may 1996, pp. 435 –441.

[42] M. Pursley and W. Stark, “Antijam capability of frequency-hop spread-spectrum with reed-solomon coding,” in *Military Communications Conference, 1983. MILCOM 1983. IEEE*, vol. 1, 31 1983-nov. 2 1983, pp. 7 –11.

[43] W. Phoel, J. Pursley, M. Pursley, and J. Skinner, “Frequency-hop spread spectrum with quadrature amplitude modulation and error-control coding,” in *Military Communications Conference, 2004. MILCOM 2004. 2004 IEEE*, vol. 2, oct.-3 nov. 2004, pp. 913 – 919 Vol. 2.

[44] M. Pursley and W. Stark, “Performance of reed-solomon coded frequency-hop spread-spectrum communications in partial-band interference,” *Communications, IEEE Transactions on*, vol. 33, no. 8, pp. 767 – 774, aug 1985.

[45] A.-G. Daraiseh and C. Baum, “Packet combining in frequency-hop spread-spectrum communication systems,” *Communications, IEEE Transactions on*, vol. 46, no. 1, pp. 23 –33, jan 1998.

[46] J. Gass, J.H. and M. Pursley, “Intersymbol interference in slow-frequency-hop spread-spectrum transmission over frequency-selective fading channels,” in *Information Theory, 1998. Proceedings. 1998 IEEE International Symposium on*, aug 1998, p. 455.

[47] M. Pursley and H. Russell, “Adaptive forwarding in frequency-hop spread-spectrum packet radio networks with partial-band jamming,” *Communications, IEEE Transactions on*, vol. 41, no. 4, pp. 613 –620, apr 1993.

[48] G. Stuber and K. Yang, “Throughput analysis of a slotted frequency-hopped spread spectrum multiple access network,” in *Communications, 1989. ICC ’89, BOSTONICC/89. Conference record. ’World Prosperity Through Communications’, IEEE International Conference on*, jun 1989, pp. 494 –498 vol.1.

[49] G. Cherubini and W. Stark, “Capacity of coherent frequency-hop spread-spectrum communications,” in *Communications, 1993. ICC ’93 Geneva. Technical Program, Conference Record, IEEE International Conference on*, vol. 1, may 1993, pp. 458 –462 vol.1.

[50] C. Baum and M. Pursley, “Bayesian erasure techniques for frequency-hop spread-spectrum communications with fading and partial-band interference,” in *Spread Spectrum Techniques and Applications, 1994. IEEE ISSSTA ’94., IEEE Third International Symposium on*, jul 1994, pp. 238 –242 vol.1.

[51] M. Hegde and W. Stark, “Capacity of frequency-hop spread-spectrum multiple-access communication systems,” *Communications, IEEE Transactions on*, vol. 38, no. 7, pp. 1050 –1059, jul 1990.

[52] J. Coon, T. Macdonald, and M. Pursley, “A new method for obtaining side information in frequency-hop spread-spectrum systems,” in *MILCOM 2000. 21st Century Military Communications Conference Proceedings*, vol. 1, 2000, pp. 144 –148 vol.1.

[53] C. M. Keller and M. B. Pursley, “Diversity combining for frequency-hop spread-spectrum communications with partial-band interference,” in *Military Communications Conference, 1984. MILCOM 1984. IEEE*, vol. 3, oct. 1984, pp. 464 –468.

[54] E. Lance and G. Kaleh, “A diversity scheme for a phase-coherent frequency-hopping spread-spectrum system,” *Communications, IEEE Transactions on*, vol. 45, no. 9, pp. 1123 –1129, sep 1997.

[55] A. Hassan, W. Stark, and J. Hershey, “Frequency-hopped spread spectrum in the presence of a follower partial-band jammer,” *Communications, IEEE Transactions on*, vol. 41, no. 7, pp. 1125 –1131, Jul 1993.

BIOGRAPHICAL SKETCH

Oluwatosin A. Adeladan received the B.S. in Electrical Engineering degree from the University of Alabama at Birmingham (UAB) in 2007 and the M.S. and Ph.D. degrees in electrical engineering from the University of Florida in 2008 and 2012, respectively. His current research interests lie in the area of communication theory applied to improving the multi-user capabilities of ad-hoc and sensor networks as well as cross-layer approaches to improve throughput performance in fading channels.